



**Gesellschaft für Anlagen-  
und Reaktorsicherheit  
(GRS) mbH**

**Experimental Study of  
the Hydromechanical  
Behaviour of the  
Callovo-Oxfordian  
Argillites**

Part of the  
MODEX-REP Project



Gesellschaft für Anlagen-  
und Reaktorsicherheit  
(GRS) mbH

## Experimental Study of the Hydromechanical Behaviour of the Callovo-Oxfordian Argillites

Part of the  
MODEX-REP Project

Chun-Liang Zhang  
Jürgen Dittrich  
Jürgen Müller  
Tilman Rothfuchs

Dezember 2002

### **Anmerkung:**

This report was prepared under contract No. 02E9420 with the Bundesministerium für Wirtschaft und Technologie (BMWi) and under contract No. FIKW-CT2000-29 with the Commission of the European Communities in the fifth framework programme for research and training in the field of nuclear energy (1998-2002).

The work was conducted by the Gesellschaft für Anlagen- und Reaktorsicherheit (GRS) mbH.

The authors are responsible for the content of this report.

**GRS - 187**  
**ISBN 3-931995-55-0**

**Deskriptoren:**

Deponie, EU, Evaluierung, Geomechanik, Internationale Zusammenarbeit, Modell, Verifikation

## Foreword

The MODEX-REP project (**MOD** – **MO**deling, **EX** – **EX**periment, **REP** – **RE**sponse to shaft (**P**uits) sinking) represents a European research project performed by the French Agence Nationale Pour la Gestion de Déchets Radioactifs (ANDRA). The project focuses on the development of constitutive models describing the coupled hydro-mechanical behaviour of the Callovo Oxfordian (CO) argillite at the Meuse-Haute Marne Underground Research Laboratory (MHM/URL) in eastern France.

The project comprises four work packages including (1) the development of the constitutive models by analysing surface laboratory tests, (2) the prediction of the rock mass response to shaft sinking, (3) the analysis of the in-situ-measurement results, and (4) the validation of the developed models by comparison of the predictions with the data measured during shaft sinking.

The project is performed by ANDRA in cooperation with a group of six European partner organisations among which the Gesellschaft für Anlagen- und Reaktorsicherheit (GRS) mbH – Germany is responsible for conducting geomechanical laboratory experiments for completion of the existing data base on the hydro-mechanical behaviour of the CO argillite.

The MODEX-REP project is co-funded by the project partners and their national funding institutions, respectively, and by the Commission of the European Communities (CEC) under contract no. FIKW-CT-2000-00029.

This report summarizes the results obtained during a two years geomechanical research programme conducted at GRS's Geotechnical Laboratory in Braunschweig, Germany.

# Table of Contents

	<b>Foreword</b> .....	<b>I</b>
<b>1</b>	<b>Introduction</b> .....	<b>1</b>
1.1	Meuse/Haute-Marne Underground Research Laboratory .....	1
1.2	MODEX-REP Project .....	3
1.3	Laboratory Programme within the MODEX-REP Project .....	5
<b>2</b>	<b>Petrophysical Properties</b> .....	<b>7</b>
2.1	Samples .....	7
2.2	Petrophysical Properties .....	10
2.2.1	Definitions .....	11
2.2.2	Measurements and Results .....	12
<b>3</b>	<b>Permeability</b> .....	<b>15</b>
3.1	Testing Method .....	15
3.2	Results .....	17
<b>4</b>	<b>Short-term Mechanical Behaviour</b> .....	<b>23</b>
4.1	Testing Equipment .....	23
4.2	Uniaxial Compressive Behaviour .....	24
4.2.1	Testing Method .....	24
4.2.2	Results .....	24
4.3	Multistage Triaxial Compressive Behaviour .....	27
4.3.1	Testing Method .....	27
4.3.2	Results .....	29
<b>5</b>	<b>Long-term Mechanical Behaviour</b> .....	<b>37</b>
5.1	Creep Behaviour .....	37
5.1.1	Testing Method .....	37
5.1.2	Results .....	39
5.2	Relaxation Behaviour .....	56

5.2.1	Testing Method .....	56
5.2.2	Results .....	59
<b>6</b>	<b>Summary.....</b>	<b>63</b>
<b>7</b>	<b>References.....</b>	<b>67</b>
	List of Figures .....	71
	List of Tables .....	75

# 1 Introduction

## 1.1 Meuse/Haute-Marne Underground Research Laboratory

In the framework of a feasibility study of underground waste disposal in France, the Meuse/Haute-Marne Underground Research Laboratory (MHM-URL) (Figure 1-1) is currently being built in eastern France since 2000 /AND 97/99/00/01/. Access to the MHM-URL will be possible via two shafts: the main shaft and the auxiliary shaft. At a depth of about 490 m experimental galleries will be excavated.

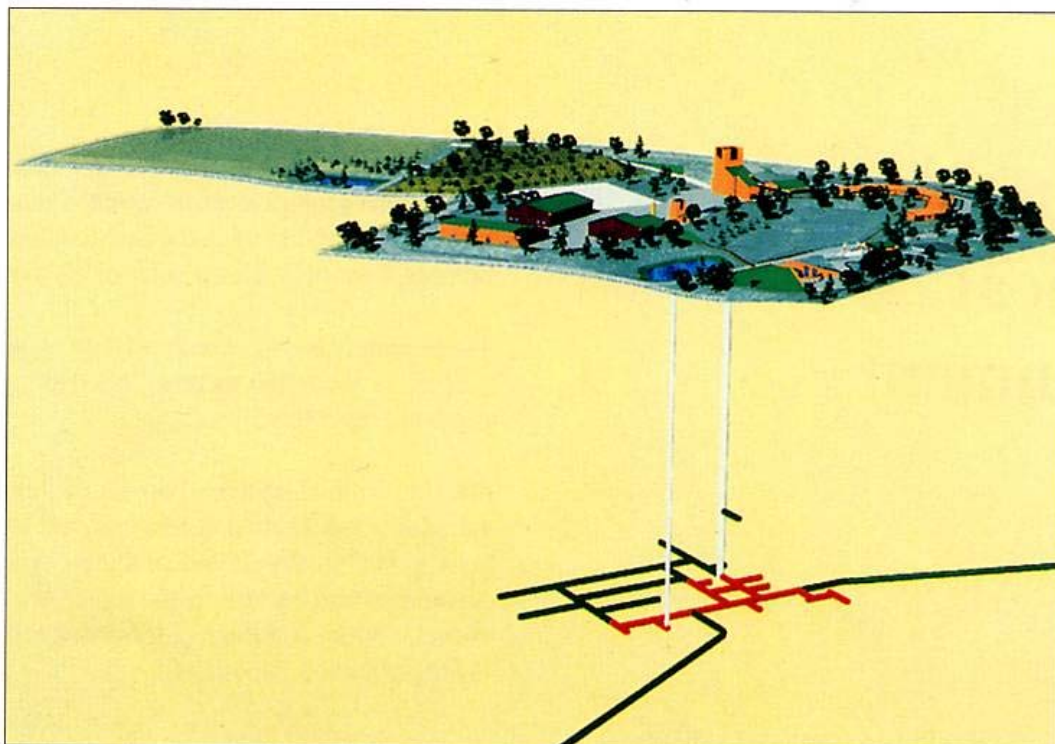


**Figure 1-1** General view of the MHM-URL in France /ANDRA 99/

The site of the MHM-URL is located within the Paris geological basin. The host formation consists of a clayey rock called Callovo-Oxfordian argillites, which is over- and under-laid by relatively impermeable carbonate formations. The argillaceous formation is located at a depth of approximately 400 m and has a thickness of 130 m. The upper part of the Callovo-Oxfordian formation will be investigated during the construction of the laboratory. Figure 1-2 shows the geological cross section of the Meuse/Haute-Marne site.

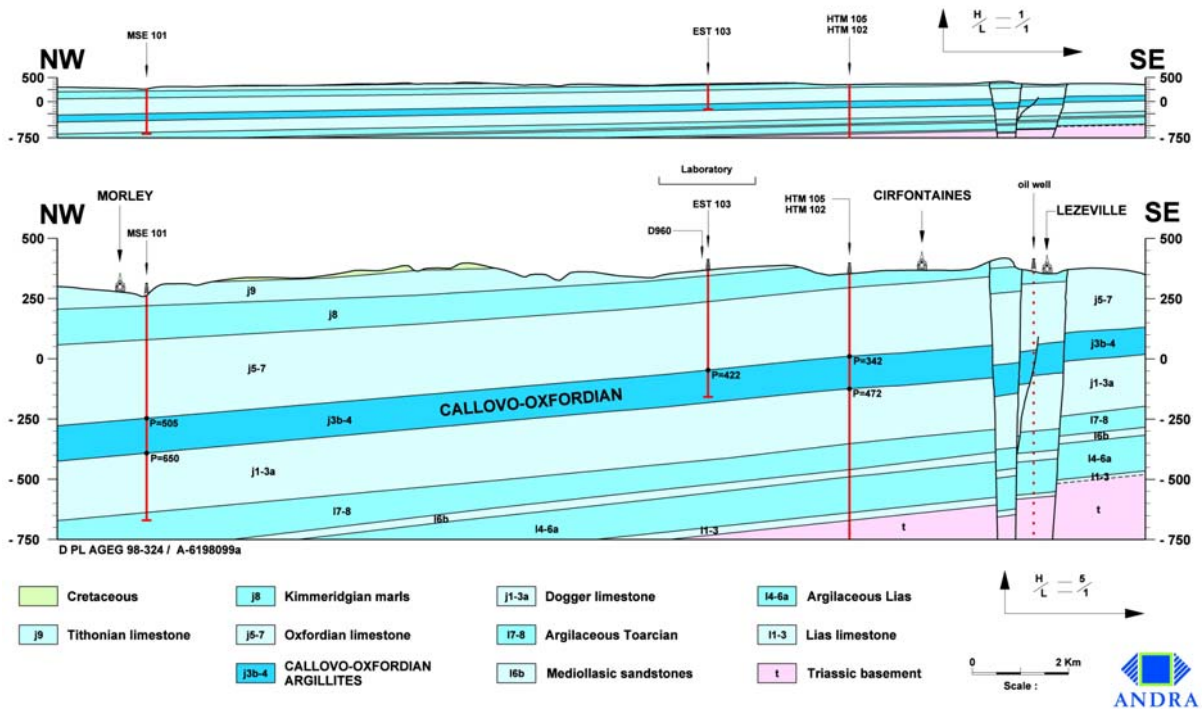


Figure 1-2 Cross section of the Meuse/Haute-Marne site /ANDRA 99/

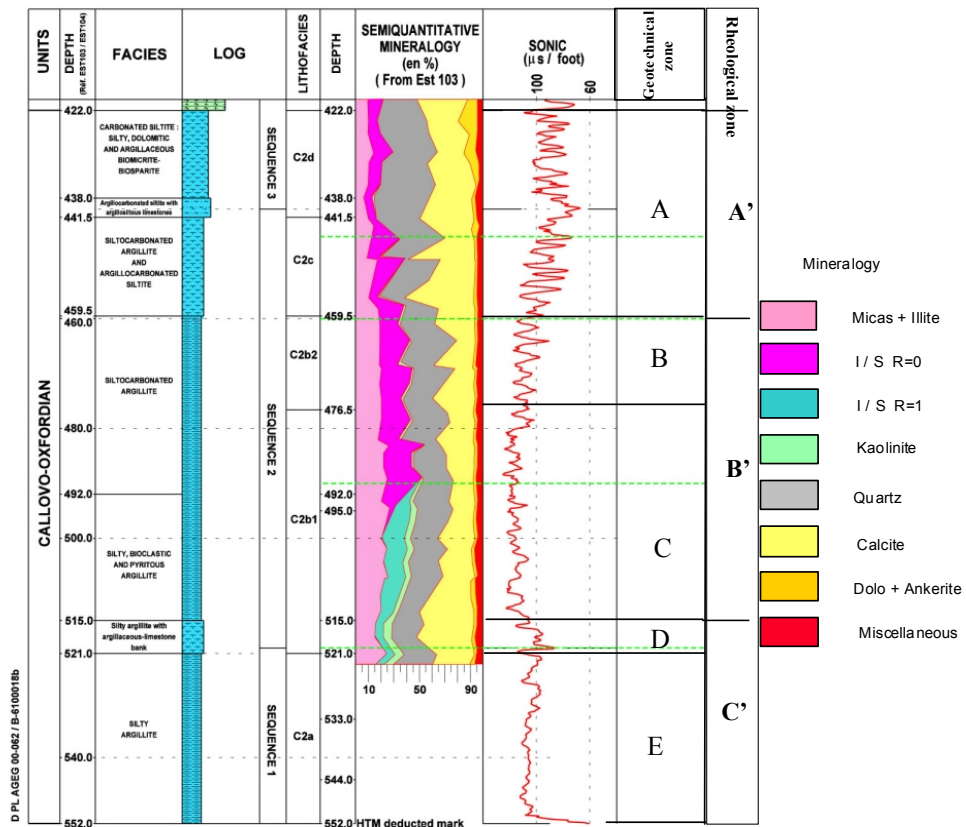


Figure 1-3 Mineralogy and geomechanical sub-division of the Callovo-Oxfordian formation /ANDRA 99/

On average the argillites contain 40 – 45 % clay minerals, 20 – 30 % carbonates and 20 – 30 % quartz and feldspar. In accordance with the mineral composition and common mechanical characteristics (strength, Young’s modulus, etc.), the host formation is divided into five geomechanical zones (A, B, C, D, E); but in terms of mechanical behaviour, three zones (A’, B’, C’) called rheological zones with significant differences of mechanical behaviour (same constitutive model applied for the three layers but with different parameters) was proposed, as illustrated in Figure 1-3. These three zones correspond to the three geological sedimentary sequences: two stiff (higher carbonate) zones surround a central less stiff (more clayey) zone. However, the transition from one zone to the other is progressive. Table 1.1 gives the main geomechanical characteristics of the host formation. Under the effect of gravity, the sedimentation of the argillites causes a preferential orientation of the clay foliation and consequently forms a stratification of the matrix structure. This results in the slight anisotropy of certain thermo-hydro-mechanical properties.

**Table 1.1** General mechanical characteristics of the Callovo-Oxfordian formation /SU 02/

Rheological zone	Thickness (m)	Density (g/cm <sup>3</sup> )	Water content (%)	Young’s modulus (MPa)	Uniaxial comp. strength (MPa)
A’ - Upper	35	2.42±0.05	6.1±1.5	5837±2455	27.0±9.5
B’- Middle	60	2.42±0.05	7.1±1.0	4723±1218	19.0±3.2
C’- Lower	35	2.46±0.05	5,9±0.7	6118±1550	21.0±3.6

## 1.2 MODEX-REP Project

In order to study the suitability of the Callovo-Oxfordian formation as a geological host formation for the disposal of high-level and long lived radioactive wastes, a set of full-scale thermo-hydro-mechanical experiments is envisaged in the MHM-URL /AND 00/, /HOT 00a/, /OZA 00/, /LEB 00/. The first one of them, called **REP** experiment (**RE**sponse to shaft (**P**uits) sinking), is a vertical Mine-by-Test in the main shaft for following the progress of the hydromechanical perturbation. The shaft will be excavated by the drill and blast method and will go as deep as 508 m. The REP experiment involves the excavation of a niche at level -445 m for drilling boreholes, to be instrumented for tracking of the disturbance before, during and after the shaft sinking from -445 m to -490 m (Figure 1-4).

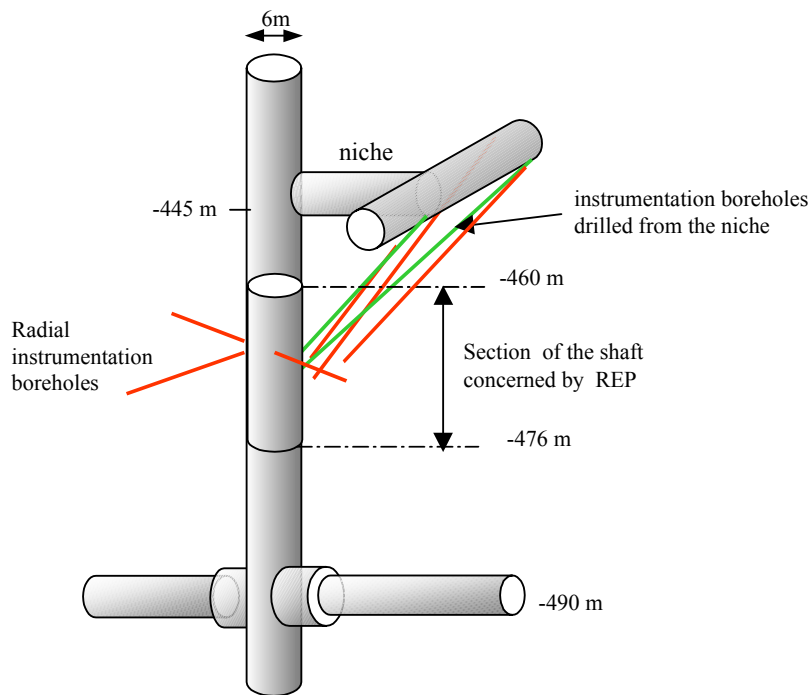


**Figure 1-4** Schematic of the REP experiment in the main shaft of the MHM-URL /SU 02/

The three main objectives of the REP experiment are:

1. Observation of the hydromechanical response of the argillites to the sinking and construction of the shaft,
2. Characterisation of the amplitude and extension of hydromechanical perturbation induced by sinking,
3. Testing of the capacity of existing constitutive models and numerical tools to predict the induced perturbation, improving the pertinence of the models in order to prepare the envisaged in-situ experiments in the galleries of the MHM-URL.

The latter task is sponsored by the Commission of the European Communities (CEC) within the EU project entitled “Elaboration of hydromechanical coupled models by interpretation of the disturbances observed during the sinking of the main shaft of an underground laboratory in Eastern France” (FIKW-CT-2000-00029). This project, also

called **MODEX-REP** (**MOD** – **MOD**elling, **EX** – **EX**periment, **REP** – **RE**sponse to shaft sinking), was started in October 2000 /OZA 99/00/, /SU 02/.

The MODEX-REP project consists of:

- developing constitutive models by analysing surface laboratory test results;
- predicting the rock mass response due to shaft sinking;
- analysing the results of in-situ measurements;
- comparing predicted with measured rock mass response;
- validating the models.

Accordingly, the project is divided into five work-packages (WPs):

WP 1: Analysis of geomechanical data and development of constitutive models;

WP 2: Study of the capability of constitutive models and numerical models;

WP 3: Predictive modelling of rock mass response to Mine-by-Test;

WP 4: Comparison between modelling and in-situ experiment;

WP 5: Lessons drawn from the comparison.

The project is managed by the Project Coordinator, ANDRA – the French National Agency for Radioactive Waste Management. The participants in the project are: ANDRA, COB, G3S, LML, ARMINE-CGES, ENSMP-CGES and ITASCA of France; GRS of Germany; SCK.CEN of Belgium; NAGRA of Switzerland; ENRESA and CIMNE of Spain.

### **1.3 Laboratory Programme within the MODEX-REP Project**

Since 1994, a series of laboratory experiments have been conducted on drilling cores from the Callovo-Oxfordian argillites by research partners of ANDRA, in order to characterise their thermo-hydro-mechanical behaviour /HEI 88/, /SU 99/. From the test results obtained on about 1000 samples, a database of geomechanical characteristics and parameters for clays is established and used to develop constitutive models for the Callovo-Oxfordian argillites in the MODEX-REP project. For the precise determination of model parameters for the special location of the REP-experiment, additional

laboratory experiments are necessary. Therefore, a laboratory programme was planned in the MODEX-REP project.

The main tasks of the laboratory programme are:

- Measurements of petrophysical properties of the Callovo-Oxfordian argillites, such as density, porosity and water content;
- Triaxial compression tests to examine the short-term mechanical behaviour of the clay rock, such as stress-strain-behaviour, deformation modulus and strength;
- Uniaxial creep and relaxation tests to study the long-term mechanical behaviour of the clay rock, such as viscoplastic deformation, creep rate and stress relaxation;
- Permeability measurements to characterise the hydrological properties of the host rock.

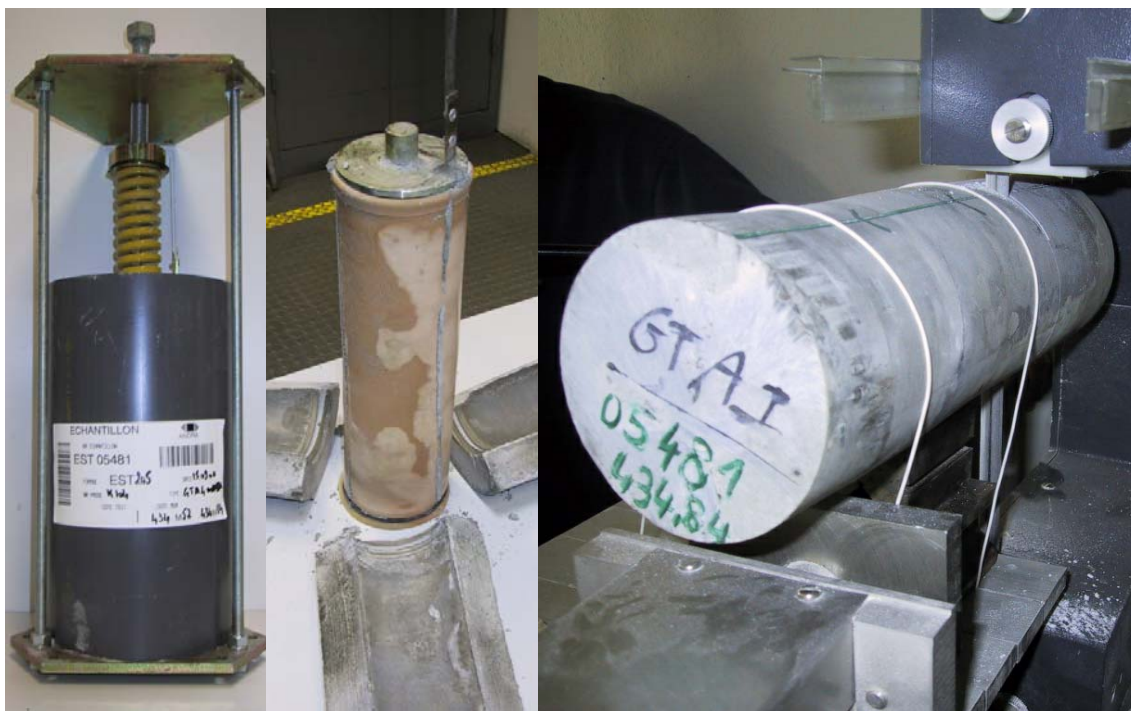
The laboratory programme was performed by GRS from October 2000 to April 2002. In this report, the results of GRS's laboratory experiments are presented.

## 2 Petrophysical Properties

### 2.1 Samples

Seven core samples of 100 mm diameter and 320 mm length were taken at different depths between 434 and 506 m of the borehole EST205, drilled at the axis of the auxiliary shaft of the MHM-URL /AND 01/, /SU 02/. They cover the two rheological zones A' and B' of the Callovo-Oxfordian formation: EST05481 from zone A' and the others from zone B'. Most of the samples originate from the same depths as the REP experiment (Figure 1-4, Table 2-1).

In order to prevent loss of water and possible damages, the samples after drilling were stored in sealing cells (Figure 2-1 A) consisting of a rubber jacket (Figure 2-1 B), an expansive mortar and a PVC-tube. In axial direction a certain load was applied by using steel headers and springs (Figure 2-1 A-B; details in /LEB 96/).



A

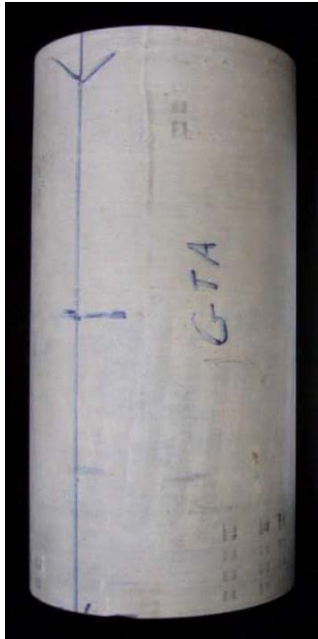
B

C

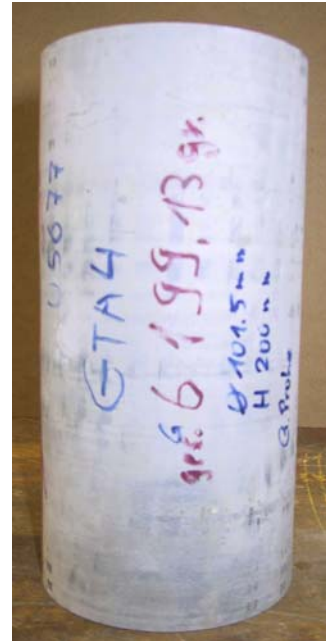
**Figure 2-1** Sample EST05481 of the Callovo-Oxfordian argillites from the borehole EST205 in the GRS laboratory under storage conditions and during specimen preparation



EST05481  
(434.52-434.84m)



EST05582  
(463.17-463.49m)



EST05677  
(487.05-487.37m)



EST05547 (segmented)  
(454.38-454.70m)



EST05630  
(474.00-474.32m)



EST05751  
(505.65-505.97m)

**Figure 2-2** Core samples taken from the Callovo-Oxfordian argillites from the borehole EST205

**Table 2.1** Test plan for laboratory tests on core samples taken from the Callovo-Oxfordian argillites at MHM-URL

Core No.	Depth (m)	Specimen No.	Diameter D (mm)	Length L (mm)	Experiment			
					Creep	Relaxation	Compression	Permeability
EST-05481	434.52	EST05481-01-II*	100	200	x			
	–	EST05481-02-II	40	80				x'
	434.84	EST05481-03-II	40	80				x'
		EST05481-04-II	40	80				x'
EST-05547	454.38	EST05547-01-=-*	40	80				x
	–	EST05547-02-=-	40	80				x
	454.70	EST05547-03-=-	40	80				x
		EST05547-04-=-	40	80				x
		EST05547-05-II	40	80				x
		EST05547-06-II	40	80		x	x	
		EST05547-07-II=	40	80		x'		
EST-05582	463.17	EST05582-01-II	100	200	x			
	–	EST05582-02-II	45	90	x			
	463.49	EST05582-03-II	45	90	x			
EST-05630	474.00	EST05630-01-II	100	200	x			
	–	EST05630-02-=-	45	90	x			
	474.32	EST05630-03-=-	40	80		x'		
EST-05671	484.05	EST05671-01-II	100	180	x			
	–	EST05671-02-=-	45	90	x			
	484.37	EST05671-03-=-	45	90	x			
EST-05677	487.05	EST05677-01-II	100	200	x		4x50/98	
	–	EST05677-02-II	40	80		x	x	
	487.37	EST05677-03-II	40	80		x	x	
		EST05677-04-II	40	80		x	x	
EST-05751	505.65	EST05751-01-II	100	200	x		4x50/98*	
	–	EST05751-02-II	40	80				x
	505.97	EST05751-03-II	40	80				x
		EST05751-04-II	40	80				x'

II\*: specimen axis perpendicular to the bedding; =\*: specimen axis parallel to the bedding plane; **x** : specimens tested and their data available; x': specimens or test data not available due to technical problems; 4x50/98: four specimens with D/L=50/98 mm taken from the large one after creep; 4x50/98\*: four specimens with D/L=50/98 mm not preparable from the large one.

After unpacking, no visual damages of the samples were recognised. Generally, the studied rock is a very compact material of relatively homogeneous structure and with insignificant bedding planes (Figure 2-2). From the core samples, cylindrical specimens with different sizes for different tests were very carefully prepared by cutting from the cores and polishing their end faces. After preparation the specimens were directly placed in the respective testing apparatus and the rest pieces of the samples were stored in a container for later use. The storage condition was room temperature of  $20\pm 2^{\circ}\text{C}$  and constant relative air humidity of 94 %, which corresponds to the value determined on the undisturbed delivered samples at  $20^{\circ}\text{C}$ .

The samples were planned for a series of hydromechanical experiments as given in Table 2.1. In summary, the following tests were foreseen:

- Uniaxial creep tests: six large specimens of 100 mm diameter and 200 mm length with the axis perpendicular to the bedding plane; five small ones of D/L = 45/90 mm, two of them perpendicular to the bedding plane and the three others parallel.
- Uniaxial compression and relaxation tests: six specimens of D/L = 40/80 mm, four of them perpendicular to the bedding plane and the two others parallel (the last two ones failed).
- Triaxial compression tests: eight specimens of D/L = 50/98 mm with the axis perpendicular to the bedding plane, taken from the large specimens (D/L = 100/200 mm) used in the creep tests, four small specimens (D/L = 50/98 mm) from the core EST05677, but four specimens from the core EST05751 were not preparable.
- Gas permeability tests: eleven specimens of D/L = 40/80 mm, seven of them with the axis perpendicular to the bedding plane and four parallel (four tests failed).

## **2.2 Petrophysical Properties**

Hydromechanical behaviour of clays is very linked to their petrophysical properties such as mineralogical composition, density, porosity, water content etc.. In addition, petrophysical characterisation is being used for the classification of clay formations and the definition of hydromechanically homogeneous zones. According to ISRM suggested testing methods /ISR 81/, the following properties of the Callovo-Oxfordian

argillaceous samples were measured and determined: grain density, bulk density, porosity and water content.

### 2.2.1 Definitions

The above mentioned physical properties are defined as below /ISR 81/:

- Grain density 
$$\rho_s = \frac{M_s}{V_s} \quad (2.1)$$

with  $M_s$  = mass of solids,  $V_s$  = volume of solids.

- Bulk density 
$$\rho_b = \frac{M}{V} = \frac{M_s + M_w}{V} \quad (2.2)$$

with  $M$  = mass of bulk sample,  $V$  = volume of bulk sample,  $M_s$  = mass of solids,  $M_w$  = mass of water.

- Dry density 
$$\rho_d = \frac{M_s}{V} \quad (2.3)$$

with  $M_s$  = mass of solids,  $V$  = volume of bulk sample.

- Porosity 
$$\phi = \frac{V_v}{V} 100 = \left(1 - \frac{\rho_d}{\rho_s}\right) 100 \quad (\%) \quad (2.4)$$

with  $V_v$  = volume of voids,  $V$  = volume of bulk sample,  $\rho_d$  = dry density,  $\rho_s$  = grain density.

- Water content 
$$w = \frac{M_w}{M_s} 100 \quad (\%) \quad (2.5)$$

with  $M_w$  = mass of "free" water,  $M_s$  = mass of solids (including adsorbed water).

- Degree of saturation 
$$S = \frac{V_w}{V_v} 100 \quad (\%) \quad (2.6)$$

with  $V_w$  = volume of "free" water,  $V_v$  = volume of voids.

- Relationship between degree of saturation and the other physical characters

$$S = \frac{w}{\rho_w} \frac{1}{\left(\frac{1}{\rho_d} - \frac{1}{\rho_s}\right)} = \frac{\rho_d w}{\rho_w \phi} 100 \quad (\%) \quad (2.7)$$

with  $\rho_w$  = density of water.

- Water content of full saturated sample ( $S = 100 \%$ )

$$w_{sat} = 100 \cdot \rho_w \cdot \left( \frac{1}{\rho_d} - \frac{1}{\rho_s} \right) \quad (\%) \quad (2.8)$$

## 2.2.2 Measurements and Results

Before starting of each test, the bulk density of the specimen was determined by measuring its volume and weight. The water content of the core samples was measured on the remains produced during specimen preparation. The specimens were stored in a container with relative air humidity of 94 % over some months and then dried in an oven at a temperature of 105°C over about 5 days. The dry density was determined according to the values of the measured bulk density and the measured water content.

Grain densities of the core samples were firstly measured on powder specimens using Beckmann's air Pycnometer (Model 930) and using room air. The powder was produced during the specimen preparation. In order to examine the effect of temperature on the grain density, powder specimens were dried in room air with the relative air humidity of about 35 % at a temperature of about 20°C and in an oven at 105°C over 3 – 10 days, respectively. The oven-dried powder specimens were isolated to air and cooled at about 20°C for 3 – 4 days. The results of the measurements are given in Table 2.2. The measured grain densities of about 2.63 g/cm<sup>3</sup> for the air-dried specimens are lower than  $\rho_s = 2.90 - 3.49$  g/cm<sup>3</sup> measured on the oven-dried ones at 105°C. The values of  $\rho_s = 2.90 - 3.49$  g/cm<sup>3</sup> obtained on the oven-dried specimens are too high, in comparison to the grain density values of 2.7 – 2.8 g/cm<sup>3</sup> for the common mineral constituents of clays /HOR 96/.

To check the high grain density values measured above, a series of controlling measurements was carried out. The first controlling test was performed on the same powder specimens using another air pycnometer (Porotec-Pycnometer) and using nitrogen gas. The measurement resulted in grain density values of  $\rho_s = 2.63$  g/cm<sup>3</sup> for the air-dried specimens and  $\rho_s = 3.27$  g/cm<sup>3</sup> for the oven-dried specimens at 105°C, which are the same as the earlier results.

**Table 2.2** Measurements of the grain density on powder specimens from the Callovo-Oxfordian argillites at MHM-UTRL using Beckmann' Pycnometer

<b>Core sample</b>	<b>Depth z (m)</b>	<b>Grain density</b> (material dried at 20°C) $\rho_{s-20}$ (g/cm <sup>3</sup> )	<b>Grain density</b> (material dried in oven at 105°C) $\rho_{s-105}$ (g/cm <sup>3</sup> )
EST05481	434.52-434.84	2.641	2.903
EST05547	454.38-454.70	2.640	3.223
EST05582	463.17-463.49	2.584	3.106
EST05630	474.00-474.32	2.583	3.357
EST05671	484.05-484.37	2.596	3.212
EST05677	487.05-487.37	2.618	3.460
EST05751	505.65-505.97	2.660	3.492

In the second controlling test, solid specimens were used. The test resulted in grain densities of  $\rho_{s-20} = 2.41$  g/cm<sup>3</sup> for the water-saturated specimens and  $\rho_{s-105} = 3.40$  g/cm<sup>3</sup> for the oven-dried specimens at 105°C. The results are in a good agreement with the above mentioned measurements.

The third and last controlling test called “benchmark test” was performed at the Institut für Angewandte Geowissenschaften der Technischen Universität Berlin (TU Berlin). The TU Berlin used an air pycnometer ACCUPYC-1330 and helium gas, while GRS used Beckmann's Pycnometer and room air. Before starting the test, each apparatus was calibrated. After the test, each apparatus was controlled again by measuring the volume of the same calibrating steel balls. Both measurements produced comparable results of the ball volume of 21.73 cm<sup>3</sup> by TU Berlin and 21.66 cm<sup>3</sup> by GRS. Therefore, possible uncertainties of the testing apparatuses were excluded. For the benchmark test, a powder specimen from core EST05677 was dried in an oven at 105°C for 10 days and then cooled at about 20°C. Each team conducted two measurements on the same specimen. The grain density of  $\rho_s = 2.701 \pm 0.021$  g/cm<sup>3</sup> was measured by TU Berlin, whereas GRS's results remained the same as before with  $\rho_s = 3.347 \pm 0.06$  g/cm<sup>3</sup>. The measured results are quite different, which can not be explained now. Because the result of TU Berlin is more comparable to that determined on the Callovo-Oxfordian argillites by others /SU 99/, /LEB 00/, the mean grain density of  $\rho_s = 2.7$  g/cm<sup>3</sup> is accepted in this report. Based on the grain density value and the dry densities,

porosities of all the cores are determined according to equation (2.4). Then, the degree of saturation is calculated for all the cores according to equation (2.7).

Table 2.3 summarises the measurement results of the physical properties for all the core samples. Variations of the physical properties are very small from one core to another. This means, the Callovo-Oxfordian formation at the tested depth ranging from 434 m to 506 m is very homogenous. In the calculation of the degree of saturation, the application of the mean grain density to all the cores leads to too high values of saturation over 100% for some cores. But the mean value of the degrees of saturation is nearly 100%.

**Table 2.3** Petrophysical properties of the Callovo-Oxfordian argillites at MHM-URL

Core sample	Depth (m)	Bulk density (g/cm <sup>3</sup> )	Dry density (g/cm <sup>3</sup> )	Water content (%)	Porosity (%)	Degree of saturation (%)
EST05481	434.52-434.84	2.41	2.30	4.99*	15.0	76.5*
EST05547	454.38-454.70	2.39	2.22	7.45	17.8	93.0
EST05582	463.17-463.49	2.40	2.21	8.73	18.2	106.0
EST05630	474.00-474.32	2.38	2.18	8.93	19.2	101.0
EST05671	484.05-484.37	2.44	2.27	7.38	15.8	106.0
EST05677	487.05-487.37	2.43	2.27	7.10	16.1	100.0
EST05751	505.65-505.97	2.42	2.28	6.35	15.7	92.3
Mean value		2.41	2.25	7.66	16.8	99.7
Maximum deviation		±0.03	±0.05	±1.27	±2.0	±6.0

\* the water content of 4.99 % for core EST05481 was measured on desaturated specimens

### 3 Permeability

To determine the intrinsic permeability of the Callovo-Oxfordian argillites, gas permeability tests were performed under the expected in-situ conditions such as overburden pressure and material anisotropy.

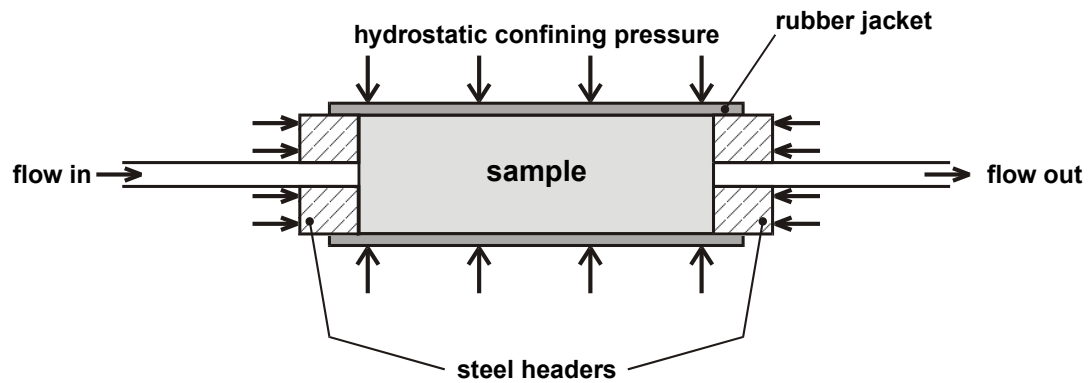
#### 3.1 Testing Method

Figure 3-1 A shows the principle of the gas permeability measurement in a pressure vessel. A specimen is inserted in a rubber jacket and two steel headers. The specimen assembly is installed in a pressure vessel in which the specimen is subjected to a confining pressure applied by fluid. Under constant confining pressure gas is injected at one end of the specimen and at the other side the gas flow rate is measured against atmospheric pressure. Thus, the gas permeability of the specimen can be determined as a function of confining pressure. The injection pressure must be always lower than the confining pressure in order to prevent leakage along the interface between jacket and specimen. Confining pressure and injection pressure are measured with pressure transducers. The gas flow rate is determined with thermal mass flow meters at higher flow rates. At lower gas flow rates they are determined by the displacement of water in a graduated burette. The accuracy of the pressure transducers is  $\pm 0.1$  % of readings and that of the mass flow meters is  $\pm 0.8$  %. The accuracy of the burettes is  $\pm 0.05$  cm<sup>3</sup>. GRS's testing apparatus (Figure 3-1 B) allows the permeability measurements to be conducted simultaneously on four independent specimens.

During steady state gas flow, the intrinsic permeability is determined using Darcy's law for compressive media /JOC 00/:

$$k = \frac{2 \cdot q \cdot \mu \cdot L \cdot p_o}{A \cdot (p_1^2 - p_o^2)} \quad (3.1)$$

where  $k$  is the intrinsic permeability (m<sup>2</sup>),  $q$  is the flow rate of the gas (m<sup>3</sup>/s),  $\mu$  is the gas dynamic viscosity (Pa·s),  $L$  is the length of the specimen (m),  $A$  is the section of the specimen (m<sup>2</sup>),  $p_o$  is the atmospheric pressure (Pa),  $p_1$  is the injection pressure (Pa).



A: measurement principle



B: testing apparatus

**Figure 3-1** Schematic of the measurement principle and the testing apparatus of gas permeability at GRS geotechnical laboratory in Braunschweig

Gas permeability of the Callovo-Oxfordian argillites was determined at ambient temperature under confining pressures  $p_c$  up to 16 MPa by using nitrogen gas as flow medium. The tests were divided into three groups:

Group I: three specimens of EST05481-02 / -03 / -04, with flowing direction perpendicular to the bedding plane;

Group II: two specimens of EST05751-02 / -03 perpendicular and one of EST05547-01 parallel to the bedding plane;

Group III: three specimens of EST05547-02 / -03 / -04 parallel and one of EST05547-05 perpendicular to the bedding plane.

The specimens were 40 mm in diameter and 80 mm long. The permeability measurements were made in two steps:

- (1) On the specimens with natural water contents: Under confining pressures of 2.4 and 3.0 MPa, nitrogen gas was injected into the specimens with a constant pressure of 1.9 MPa. During gas flow the specimens were desaturated. After reaching steady state flow, the gas permeability measurement was performed.
- (2) On the dried specimens: After terminating the first step of the measurements, the specimens were dried in an oven at 105°C for several days and their remaining water contents were determined. The gas permeability was measured again on the dried specimens under a constant injection pressure of 1.95 MPa and different confining pressures up to 16.2 MPa.

In the first group of the tests, confining pressures were applied on the specimens by using nitrogen gas. In the subsequent evaluation of the test data, it was found that the rubber jacket self and the jacket / specimen interface was not impermeable to the confining gas. The results are therefore unusable. In the further two groups of the tests, the problem was solved by using water as confining medium and by filling the jacket / specimen interface with silicone paste.

### **3.2 Results**

- Dry Samples

The results of the gas permeability tests are summarised in Table 3.1. On the dry specimens, the measurement revealed a permeability parallel to the bedding plane of  $k = 8 \cdot 10^{-19} - 1 \cdot 10^{-17} \text{ m}^2$  for low confining pressures of 2.4 – 3.0 MPa and of  $k = 5 \cdot 10^{-19} - 8 \cdot 10^{-19} \text{ m}^2$  for high confining pressures of 14.5 – 16.2 MPa, while the permeability perpendicular to the bedding plane was determined to  $k = 6 \cdot 10^{-20} - 3 \cdot 10^{-19} \text{ m}^2$  for the low confining pressures and  $k = 4 \cdot 10^{-20} - 1 \cdot 10^{-19} \text{ m}^2$  for the high confining pressures.

**Table 3.1** Results of gas permeability tests on the Callovo-Oxfordian argillites at MHM-URL

Group I: the tests failed.

Group II

Specimen		05751/02-II	05751/03-II	05547/01-=-
Flow direction to the bedding		perpendicular	perpendicular	parallel
Water content w (%)		5.30 %	5.00 %	4.20 %
Confining pressure (MPa)	Injection pressure (MPa)	Permeability (m <sup>2</sup> )		
2.4	1.8	6.7E-22	9.3E-22	9.1E-22
Water content w = 0.0 %				
2.4	1.98	5.4E-20	2.4E-19	1.4E-17
5.1	1.98	6.2E-20	1.8E-19	4.4E-18
8.8	1.96	5.5E-20	1.5E-19	1.5E-18
12.0	1.95	5.3E-20	1.0E-19	6.8E-19
12.8	1.95	5.1E-20	1.2E-19	6.6E-19
15.0	1.95	4.6E-20	1.0E-19	5.2E-19
16.2	1.95	4.9E-20	8.3E-20	5.4E-19

Group III

Specimen		05547/02-=-	05547/03-=-	05547/04-=-	05547/05-II
Flow direction to the bedding		parallel	parallel	parallel	perpendicular
Water content w (%)		3.30 %	3.70 %	4.50 %	4.60 %
Confining pressure (MPa)	Injection pressure (MPa)	Permeability (m <sup>2</sup> )			
3.0	1.93	5.1E-20	7.6E-20	4.1E-21	2.0E-22
Water content w = 0.0 %					
3.0	1.95	8.7E-19	1.1E-18	1.2E-17	1.9E-19
5.0	1.95	7.5E-19	8.9E-19		1.8E-19
6.0	1.95	9.2E-19	1.1E-18	4.5E-18	3.0E-19
9.0	1.95	8.2E-19	9.9E-19	1.8E-18	2.3E-19
12.0	1.95	7.4E-19	8.8E-19	1.1E-18	2.0E-19
14.5	1.95	6.7E-19	7.9E-19		1.7E-19

In order to clearly show the effects of confining pressure and material anisotropy, the permeability values of the dry specimens are illustrated in Figure 3-2 as a function of confining pressure and flow direction. It can be seen that the permeability decreases as

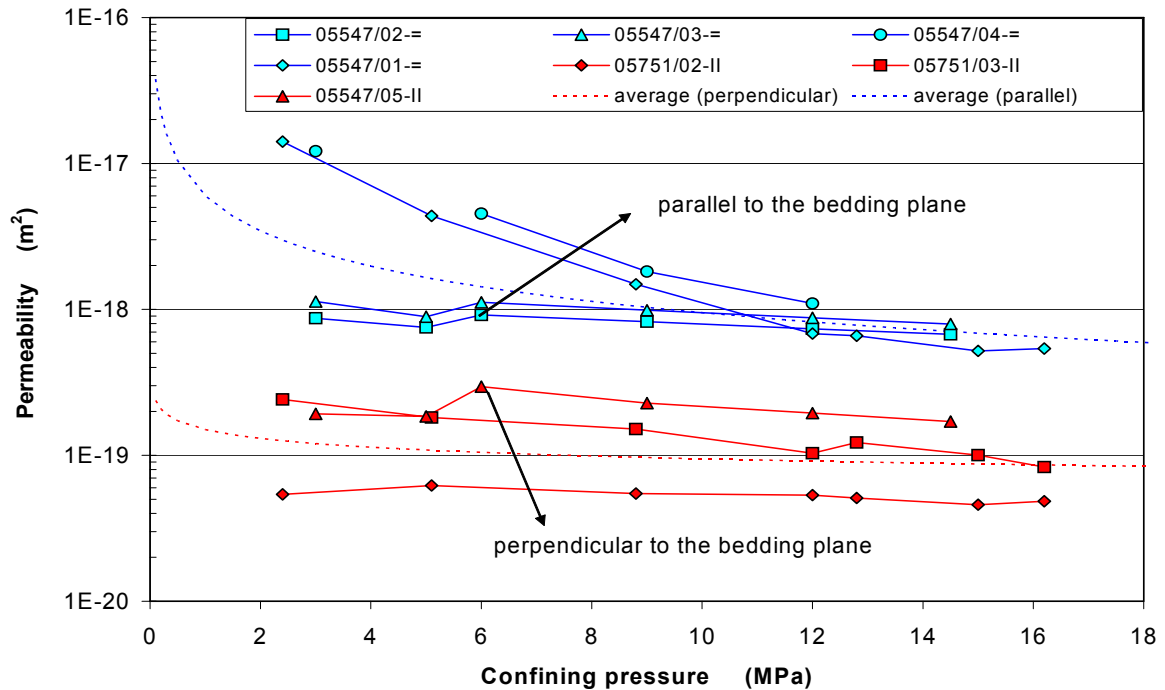


**Figure 3-2** Permeability of the Callovo-Oxfordian argillites in dependency on flow direction and confining pressure (dry specimens)

the confining pressure increases. However, independent on the flow direction the effect of the confining pressure is not very significant for most of the specimens. The ratio of the permeability for the low confining pressures  $p_c = 2.4 - 3.0$  MPa to the  $k$ -value for the high  $p_c = 14.5 - 16.2$  MPa varies between 1 to 3, except for two specimens EST05547-03 and EST05547-04 parallel to the bedding plane which show a relatively strong reduction of the permeability in the range of low confining pressures. For high confining pressures, all permeability curves parallel to the bedding plane tend to converge at the same one. This phenomenon was not observed at the specimens perpendicular to the bedding plane. Here, the difference in permeability from one specimen to another might be due to their different initial states specially such as pore connectivity etc..

On the other hand, it is obvious that in the testing range the permeability perpendicular to the bedding plane is about one order of magnitude lower than that parallel to the bedding plane. The anisotropy in permeability of the clay rock can be explained by an anisotropic pore-interconnection, existing with more intensive pore-interconnection

oriented parallel to the bedding plane and poor pore-interconnection perpendicular to the bedding plane /REN 00/.

A simple relation between intrinsic permeability  $k$  and confining pressure  $p_c$  is introduced to summarise the test data on the dry specimens:

$$k = k_o \cdot \left( \frac{p_c}{p_o} \right)^{-n} \quad (3.2)$$

where  $p_o = 1$  MPa,  $k_o$  and  $n$  are parameters. Based on the test data, the parameters are determined for the permeability of the dry Callovo-Oxfordian argillites to:

$$k_o = 1.5 \cdot 10^{-19} \text{ m}^2 \text{ and } n = 0.2$$

for the average permeability perpendicular to the bedding plane and

$$k_o = 6 \cdot 10^{-18} \text{ m}^2 \text{ and } n = 0.8$$

for the average permeability parallel to the bedding plane.

The fitting curves are illustrated in Figure 3-2 together with the test data.

- Wet Samples

Additionally, in the first step of the tests, the gas permeability was measured on the wet specimens with different water contents under low confining pressures of 2.4 – 3 MPa. The permeability values are given in Figure 3-3 as a function of water content. It is obvious that the gas permeability for the both flow directions decreases about three orders of magnitude with an increase of water content from 0 % to 4 – 5.3 %. At the high water contents, the gas permeability parallel to the bedding plane tends to that measured perpendicular to the bedding, with  $k < 1 \cdot 10^{-21} \text{ m}^2$ , too.

In comparison to other argillaceous media, the Callovo-Oxfordian argillites exhibits a typical permeability of deeply buried and compact clays in the range of  $10^{-19} - 10^{-20} \text{ m}^2$  /HOR 96/, /REN 00/. Exemplarily, the test results obtained on the dry specimens of the Callovo-Oxfordian argillites at MHM-URL are compared in Figure 3-4 with that of the marls and shales in the Swiss Central Alps /REN 00/. It is obvious that the values of the permeability perpendicular to the bedding plane are in a good agreement for all

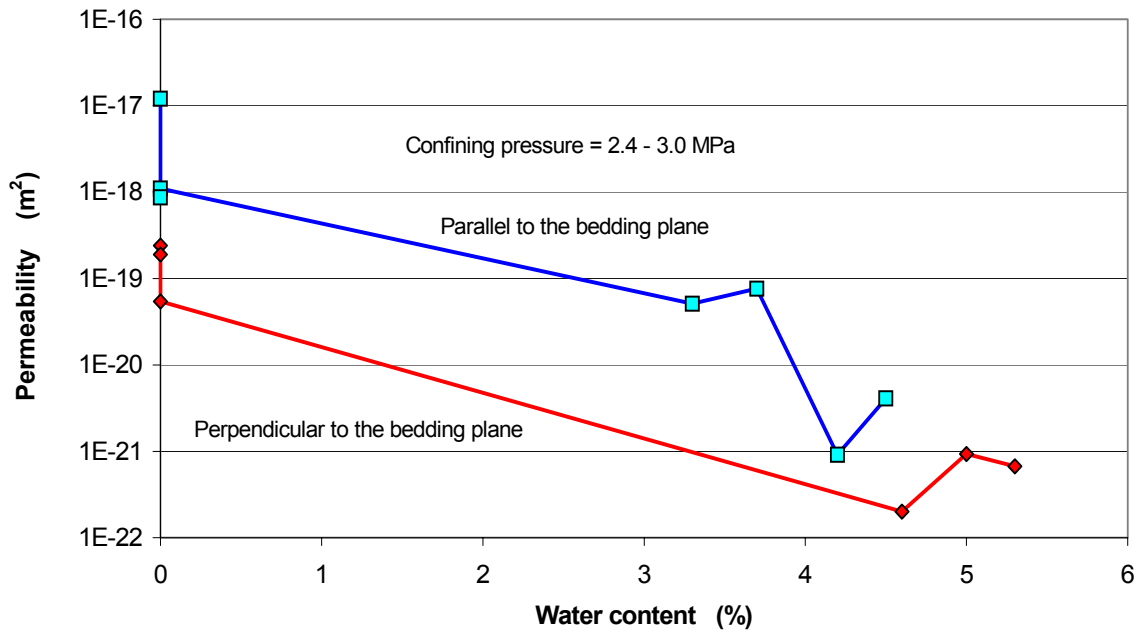


**Figure 3-3** Gas permeability of the Callovo-Oxfordian argillites in dependency on water content

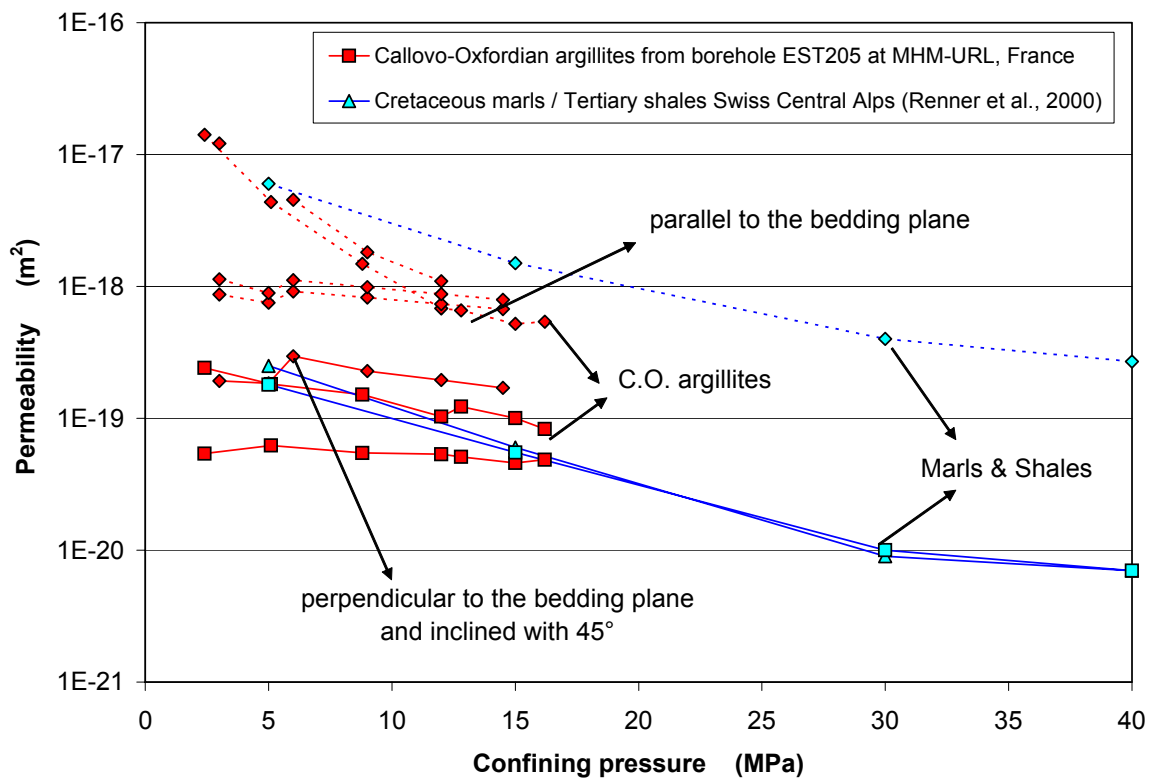


**Figure 3-4** Comparison in permeability of the Callovo-Oxfordian argillites at MHM-URL with that of the marls and shales Swiss Central Alps /REN 00/

the clays, whereas the permeability parallel to the bedding for the Callovo-Oxfordian clay rock is somewhat lower than that of the other clays. That means, the tested material taken from the Callovo-Oxfordian formation is more homogeneous than the other clays. In analogy to the results of /REN 00/, the permeability at an inclination of  $\sim 45^\circ$  to the bedding plane might be similar as that perpendicular to the bedding for the Callovo-Oxfordian argillites.

## 4 Short-term Mechanical Behaviour

In order to characterise the short-term mechanical behaviour of the Callovo-Oxfordian argillites, uniaxial and triaxial compression tests were performed on cylindrical specimens under consideration of the in-situ conditions.

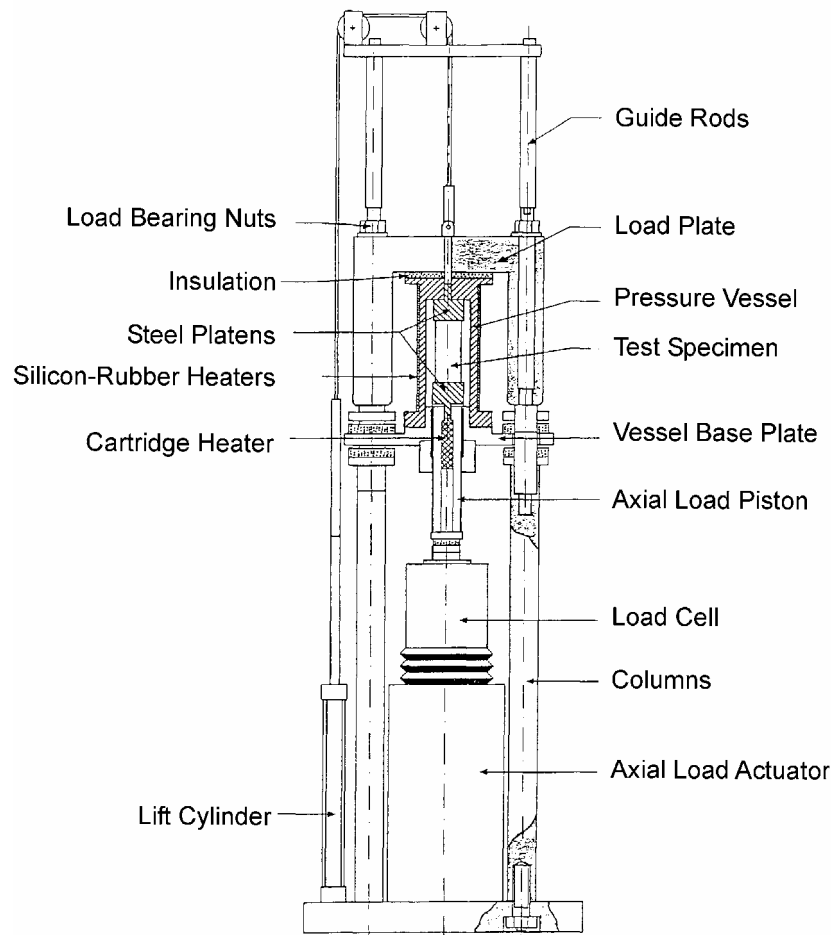


**Figure 4-1** Triaxial testing machine used at GRS geotechnical laboratory in Braunschweig

### 4.1 Testing Equipment

Uniaxial and triaxial compression experiments were conducted with a triaxial testing machine (Karman type), consisting basically of a stiff load frame and a triaxial cell, as shown in Figure 4-1. The load frame has a capacity of 1600 kN and the triaxial cell of 70 MPa. This machine allows various specimen sizes up to 100 mm diameter and 250 mm length, and a temperature up to 200°C. The axial force is measured by a load cell with an accuracy of  $\pm 0.1$  % of readings, and the cell pressure is measured by a

pressure transducer with an accuracy of  $\pm 0.1$  %. Axial deformation of the specimen is measured by a LVDT-transducer with an accuracy better than  $\pm 0.1$  %, which is installed outside of the triaxial cell between the vessel base plate and the load cell. Lateral deformation is determined from the measurement of the expelled oil volume transmitted to a pressure intensifier. The accuracy of the volume measurement is about  $\pm 100.0$  mm<sup>3</sup>, which corresponds to a volumetric strain of  $\pm 0.05$  % for the testing specimens of 50 mm diameter and 98 mm length. The machine is usually used to investigate mechanical behaviour of geomaterials at varying temperature.

## **4.2 Uniaxial Compressive Behaviour**

### **4.2.1 Testing Method**

Uniaxial compression tests were carried out on four cylindrical specimens with 40 mm diameter and 80 mm length (core EST05677 and EST05547), which were completely enclosed and sealed in rubber jackets and steel platens to prevent any change in water content during the tests. Very thin films of silicone were embedded between the ends of the specimen and the pistons to reduce the interface friction. In order to investigate the effect of water content on the mechanical behaviour, two specimens were saturated with the natural water content of 7.1 % and the other two were dried in air at ambient temperature of about 20°C, reaching a water content of 2.7 - 2.8 %. Axial load was applied to the specimens with a strain rate of  $6.5 \cdot 10^{-6}$  s<sup>-1</sup> perpendicular to the bedding plane. During the tests, multiple unloading-reloading cycles and stress relaxations were carried out in order to determine Young's modulus and the relaxation behaviour which is presented in section 5.2.

### **4.2.2 Results**

Figures 4-2 A-B illustrate the test results by comparing between the saturated and air-dried specimens. The saturated specimens reach first with the peak strength of  $\sigma_c \approx 24.0$  MPa at the corresponding deformation  $\varepsilon_{\max} \approx 1.0$  %, the stress-strain curves being nearly equal to those of the air-dried ones. After the saturated specimens ruptured, the air-dried ones deformed further, reaching a peak strength of about

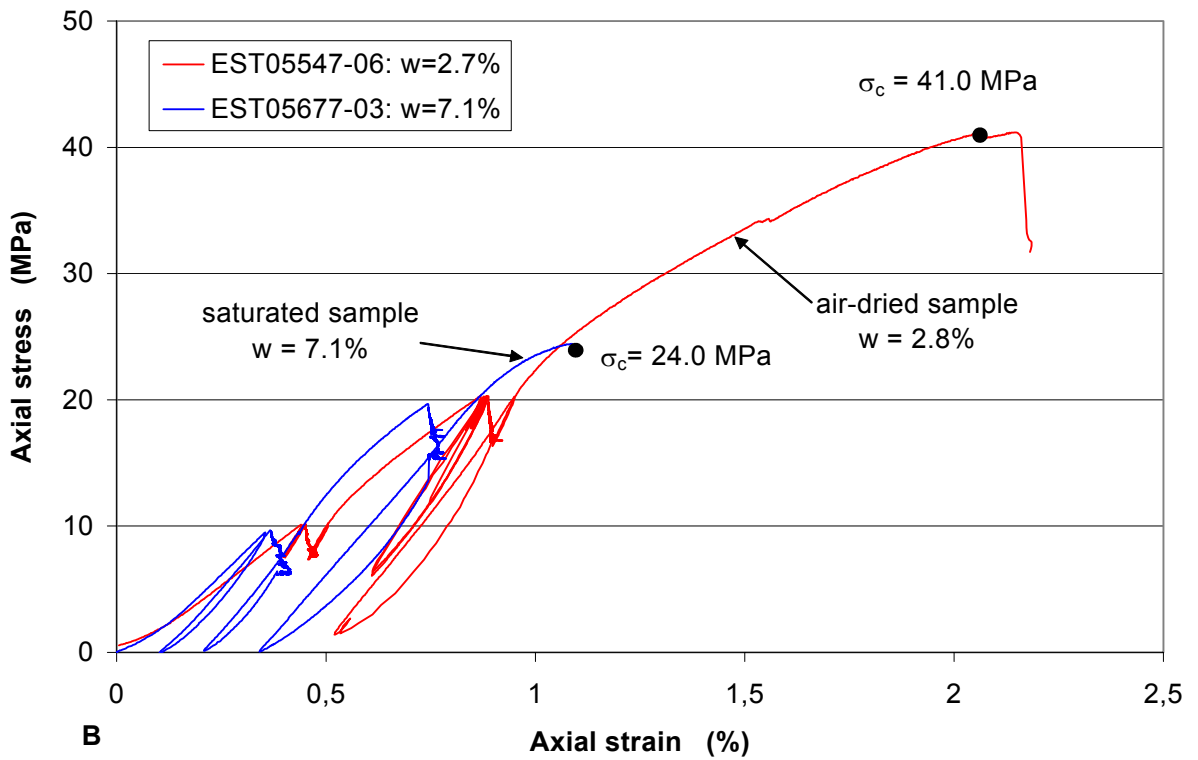
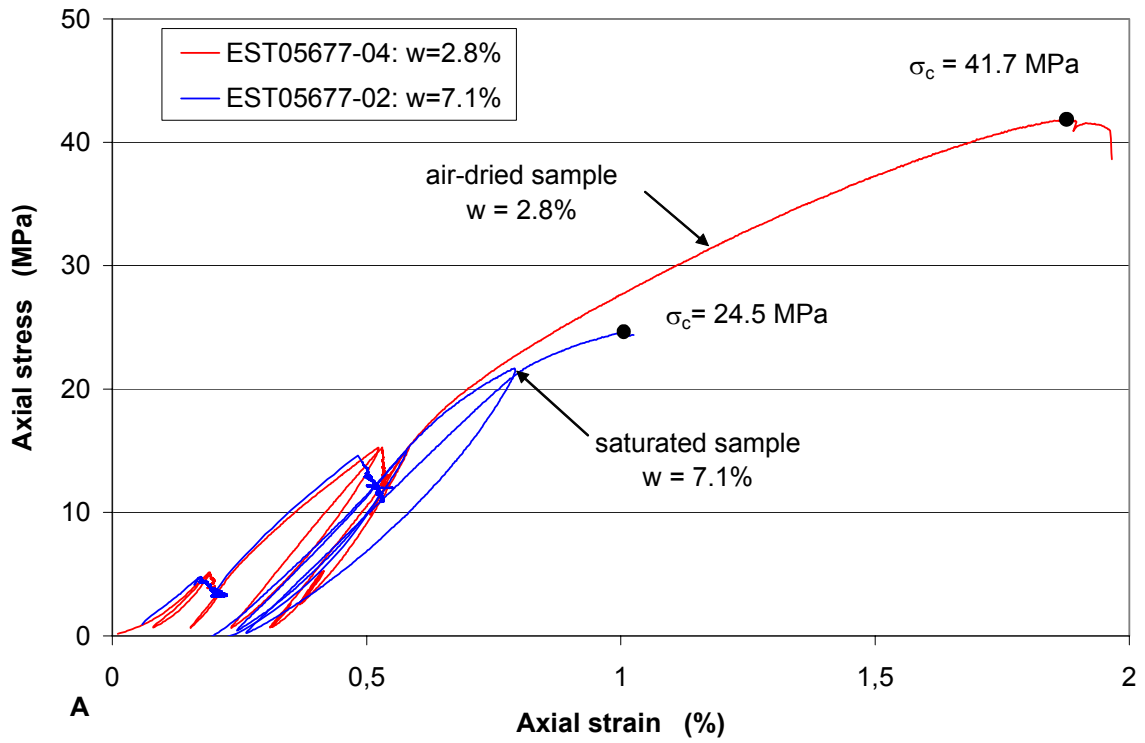


**Figure 4-2** Results of uniaxial compression tests on the specimens from the Callovo-Oxfordian argillites at MHM-URL

$\sigma_c \approx 41.0$  MPa at a deformation of about  $\varepsilon_{\max} \approx 2.0$  %. Both the peak strength and the failure deformation of the air-dried specimens are about two times larger than those of the saturated specimens. All the specimens exhibit reversible and irreversible deformation, or elasto-plastic behaviour, respectively.

Values of Young's modulus determined on the linear unloading parts of the cycles are given in Figure 4-3 as a function of load. It can be seen that the values obtained on both the saturated and the air-dried specimens vary in the same range. This means that the elastic stiffness of the clay rock is insensitive to the water content. On the other hand, the elastic modulus increases linearly from  $E \approx 5500$  MPa to  $E \approx 7500$  MPa with an increase of the axial stress from 2 MPa to 20 MPa.

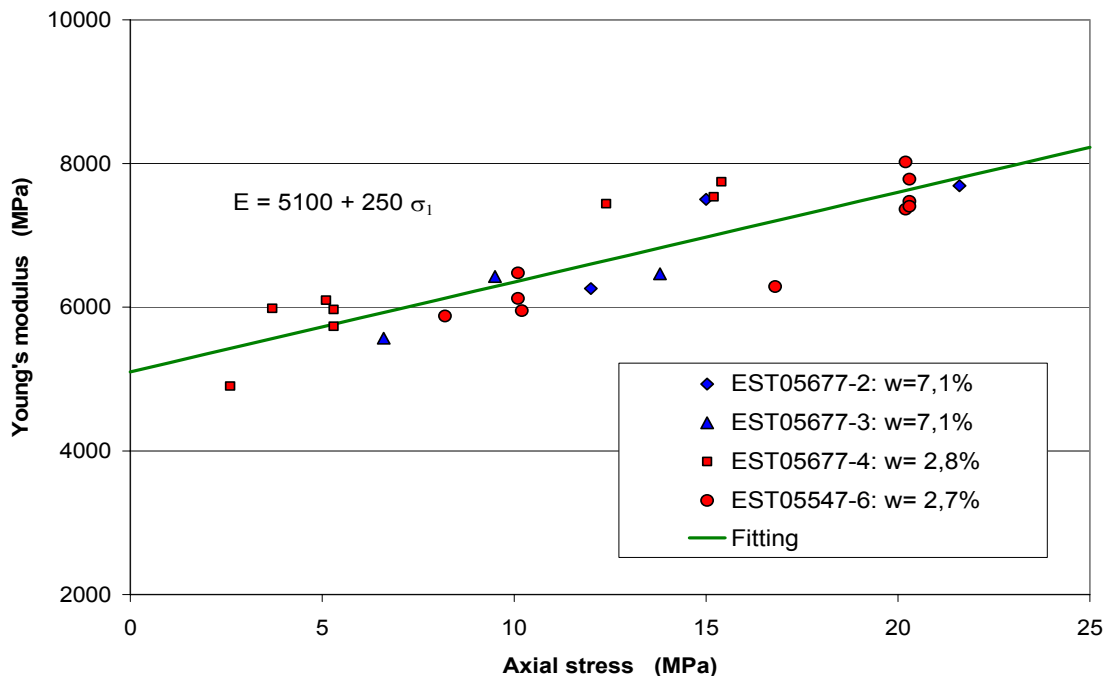


**Figure 4-3** Young's modulus as a function of axial stress (uniaxial compression tests)

Differing from the above observation, an increase of elastic stiffness with decreasing water content was reported for most clays /HOT 00b/, /SU 99/. In the triaxial compression tests on the Callovo-Oxfordian argillites done by /HOT 00b/ it was found that Young's modulus is lower when moisture content increases, but Poisson's ratio is greater. The increase of the strength and the corresponding deformation with a decrease of water content observed above is a general phenomenon for clays. In the triaxial tests by /HOT 00b/ it was also found that under a confining pressure of 10 MPa,

a decrease of the water content from 7.55 % to 4.61 % results in an increase of peak strength from  $\Delta\sigma_{\max} = (\sigma_1 - \sigma_3)_{\max} = 32$  MPa to 51 MPa at an axial deformation from  $\varepsilon_{1-\max} = 1.5$  % to 1.8 %.

In addition to the uniaxial compression tests, the elastic modulus was also determined in uniaxial creep tests (see section 5.1) in which reversible elastic and irreversible viscoplastic deformation were analysed during unloading-reloading cycles of the creep load. Figure 4-4 gives some stress-strain curves measured in creep tests on large specimens of 100 mm diameter and 200 mm length and on small specimens of D45/L90 mm perpendicular and parallel to the bedding plane. On the reloading parts of cycles Young's moduli were determined. The values are depicted in Figure 4-5 as a function of axial load. It is obvious that the elastic moduli of 4000 – 5000 MPa measured on the small specimens are more than two times higher than those of about 2000 MPa measured on the large specimens, and secondly, the stiffness in the direction parallel to the bedding plane is up to 1.5 times larger than that perpendicular to the bedding. Both, the scale effect and the anisotropy of the elastic deformation might be deduced from different distributions of microcracks in the specimens /REN 00/. However the values obtained on the large specimens are probably more realistic for the in-situ conditions.

Additionally, comparing Figures 4-2 and 4-4, it can be found that at the same loads the deformations reached in the long-term creep are larger than in the short-term compression. It should be noted here that the creep deformations reached at the time of writing this report are not finished yet, but continue for a longer time. Young's moduli determined on the reloading parts in the long-term creep tests are slightly lower than those obtained on the unloading parts in the short-term compression tests.

### **4.3 Multistage Triaxial Compressive Behaviour**

#### **4.3.1 Testing Method**

In order to gain extensive mechanical characterisations from a single test specimen, multistage triaxial compression tests were conducted within GRS's MODEX-REP laboratory programme. The principle of the multistage triaxial compression tests is: The

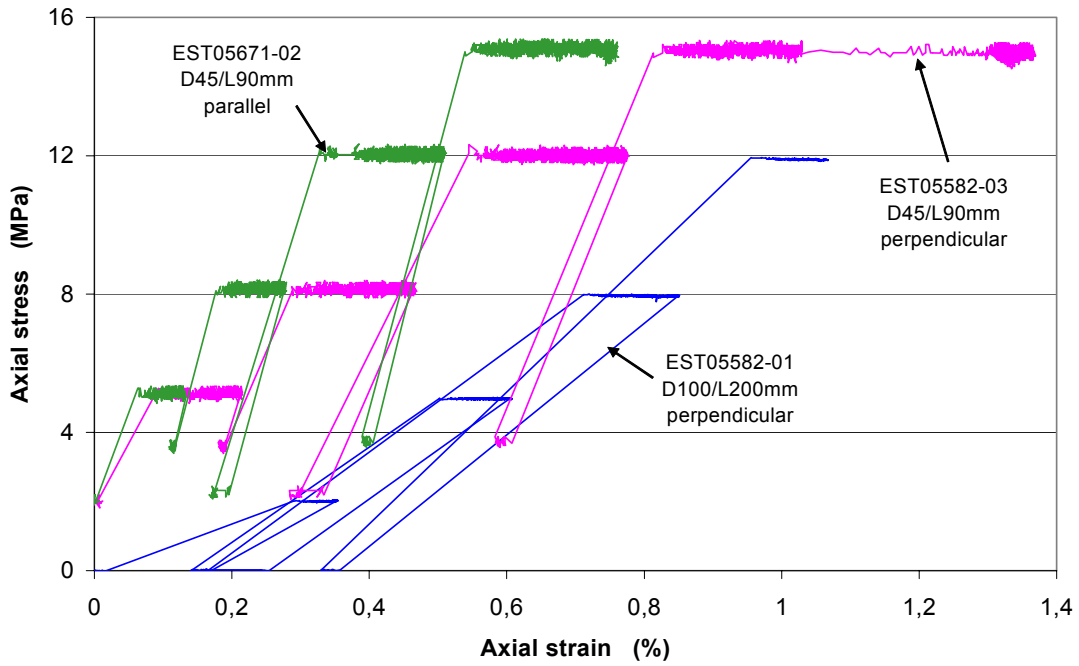


**Figure 4-4** Stress-strain curves obtained from uniaxial creep tests

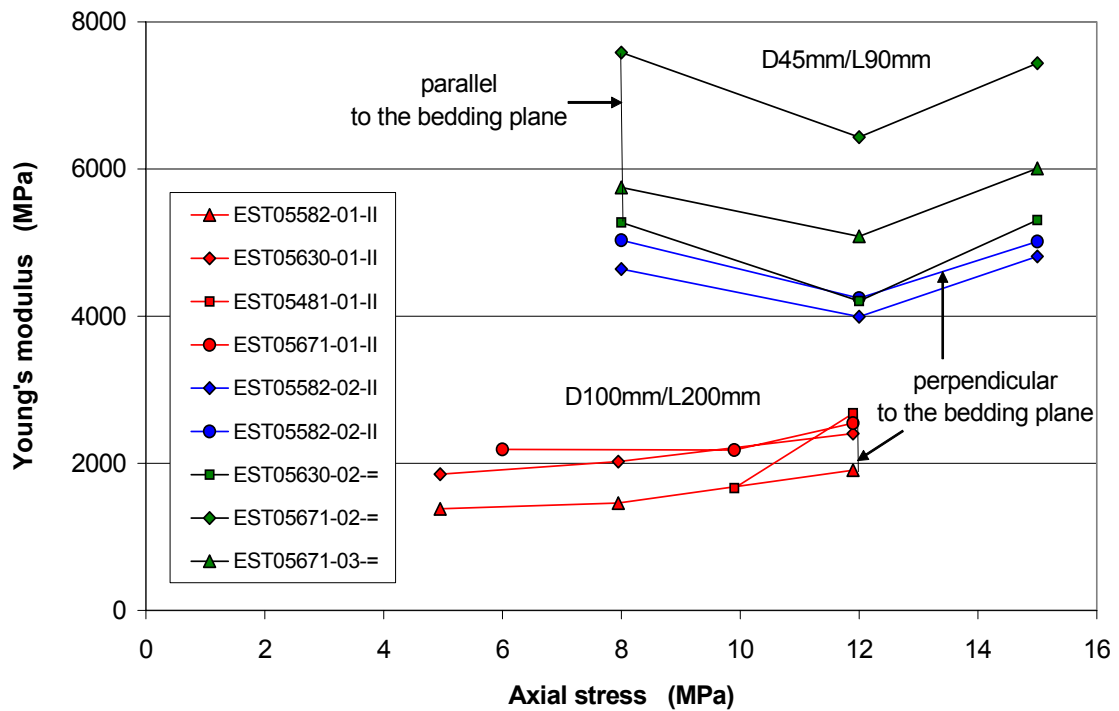


**Figure 4-5** Young's modulus as a function of axial stress (uniaxial creep tests)

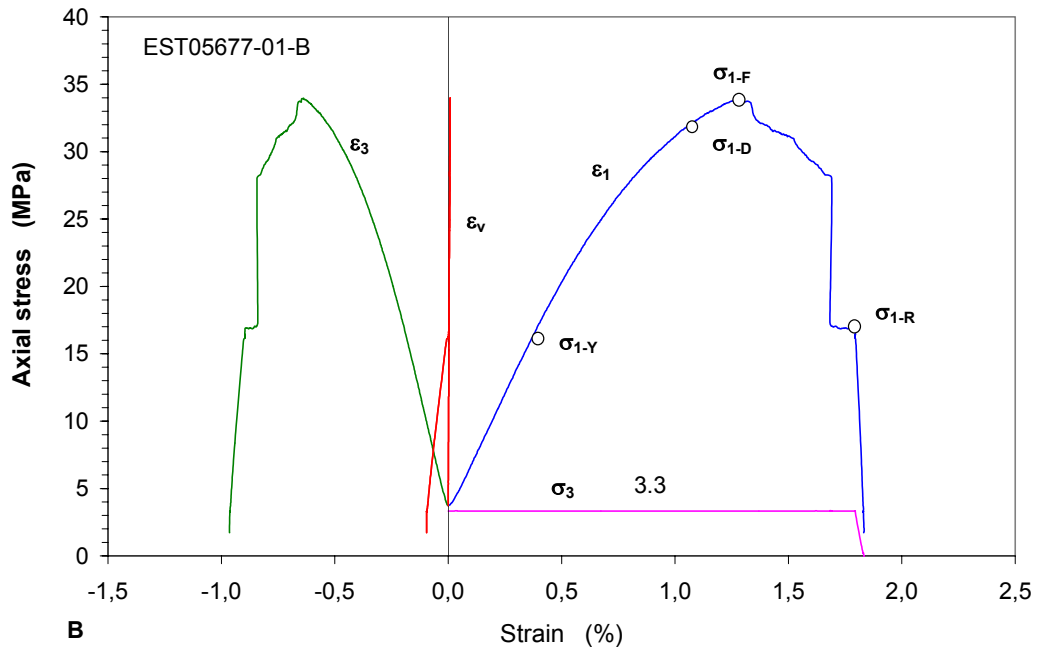
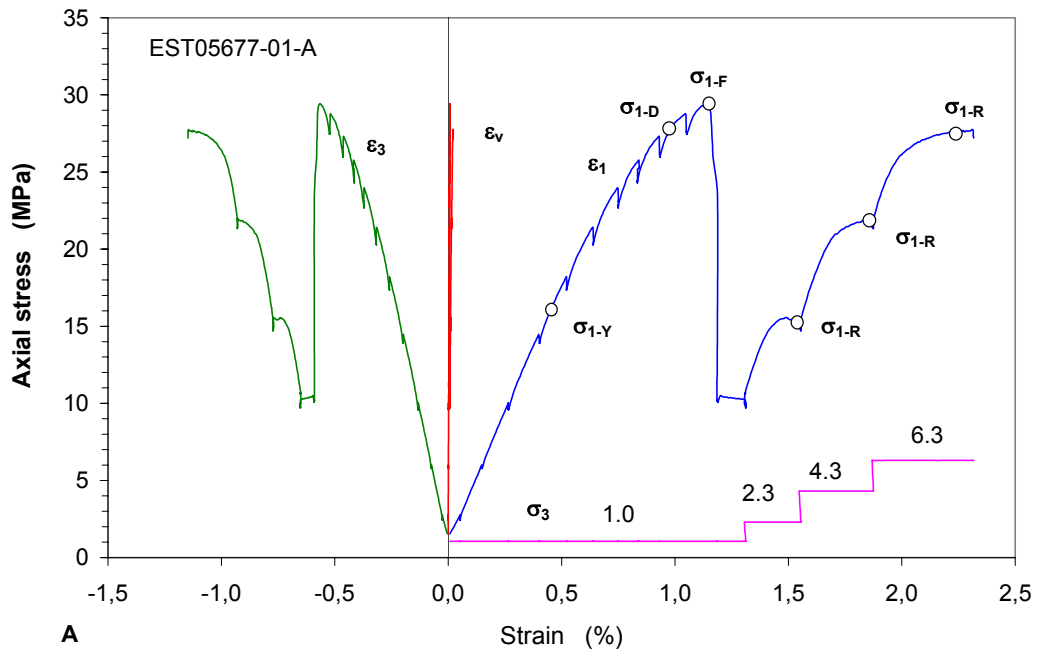
axial load is applied to the specimen under a first confining pressure until the load-strain curve indicates nearly reaching of the axial peak strength; then the confining

pressure is raised to a second value and compression of the specimen is resumed. By repeating this process one can determine damage and failure at different confining pressures. After the final stage, the axial stress and the confining pressure are reduced, respectively, but the reduction of the axial stress is done first before the confining pressure is reduced in order to maintain the stability of the specimen. The stresses are adjusted so that the specimen deforms at a relatively constant rate. The deviatoric stress maintained is defined as the residual strength. By repeating the stress reduction down to the desired levels, one can obtain residual strengths at different confining pressures from a single specimen. Figure 4-6 C gives a typical example of the multistage triaxial compression test. In literature only some multistage triaxial tests on soft soils are reported which were performed only in pre-failure stages by increasing the confining pressure, such as the tests done by /BRO 97/.

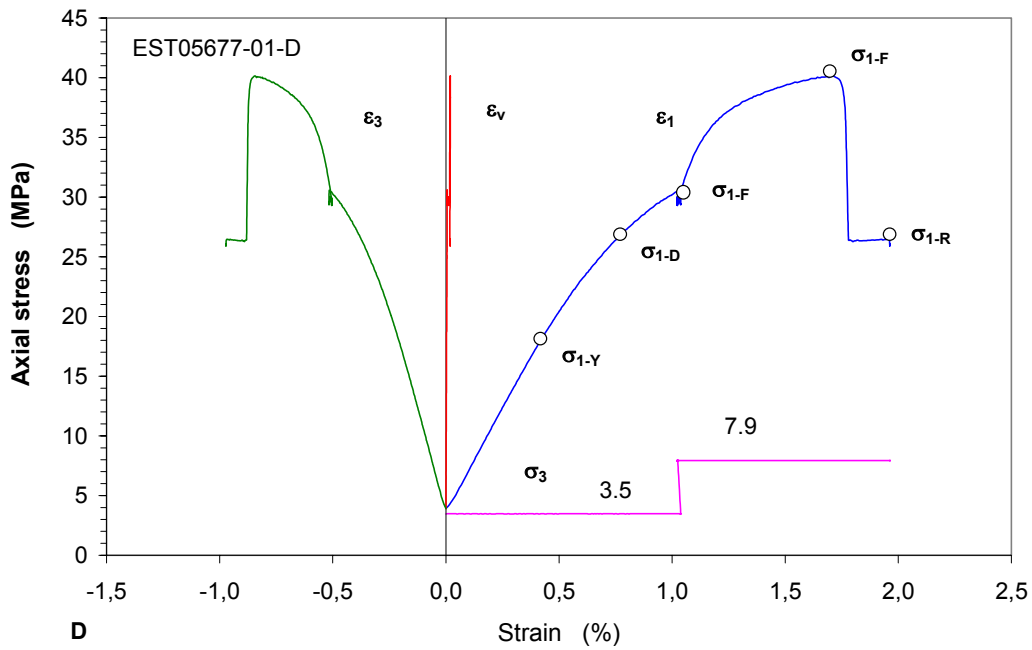
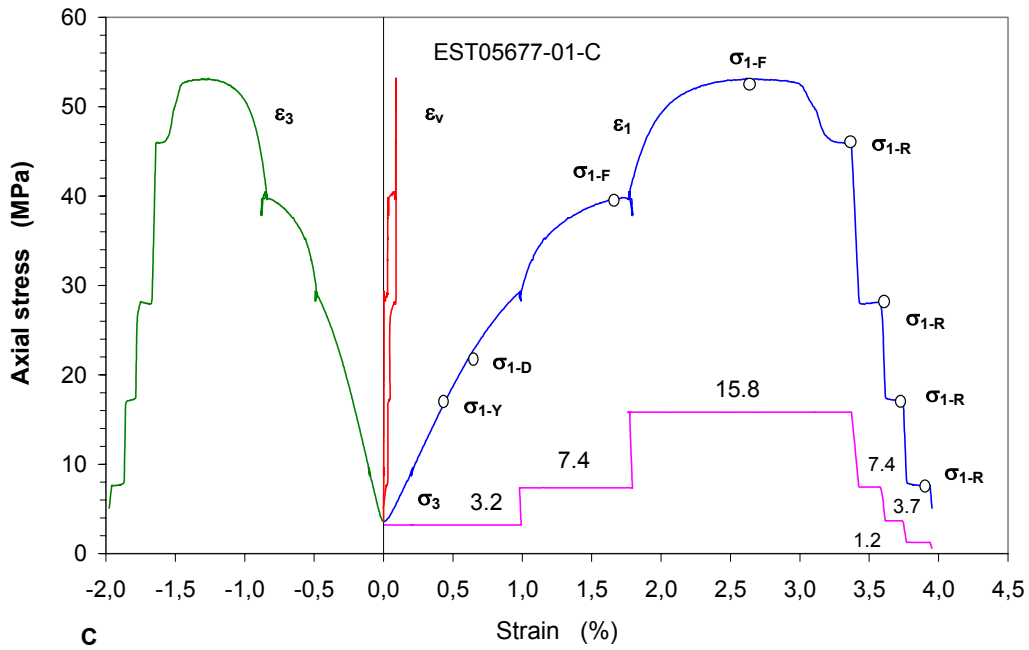
Eight specimens with 50 mm diameter and 98 mm length were originally planned for triaxial compression tests. However, the core EST05751 (depth of 505.7 m) was not compact enough for further preparation, only four specimens from the core EST05677-01 (487.15 m depth) were available for the triaxial tests. The specimens had been deformed up to 0.45 % under 4.95 MPa in creep tests performed before (see Figure 5-4). The specimens saturated with a water content of 7.1 % were completely enclosed and sealed in rubber jackets and steel platens to prevent any change in water content during the tests. Very thin films of silicone were embedded between the ends of the specimen and the pistons to reduce the interface friction. Axial load was applied to the specimens with a strain rate of  $6.5 \cdot 10^{-6} \text{ s}^{-1}$  perpendicular to the bedding plane. Different confining pressures of 0 – 16 MPa were chosen in correspondence to the in-situ conditions.

### 4.3.2 Results

Figures 4-6 A-D show the plots of axial stress – axial strain ( $\sigma_1 - \varepsilon_1$ ), axial stress – lateral strain ( $\sigma_1 - \varepsilon_3$ ), axial stress – volumetric strain ( $\sigma_1 - \varepsilon_v$ ) and confining pressure – axial strain ( $\sigma_3 - \varepsilon_1$ ) for each of the multistage triaxial compression tests.



**Figures 4-6 A-B** Results of multistage triaxial compression tests on the specimens from the Callovo-Oxfordian argillites at MHM-URL



**Figures 4-6 C-D** Results of multistage triaxial compression tests on the specimens from the Callovo-Oxfordian argillites at MHM-URL

On the axial stress – axial strain curves, axial yield stress  $\sigma_{1-Y}$ , onset of dilatancy  $\sigma_{1-D}$ , peak failure  $\sigma_{1-F}$  and residual strength  $\sigma_{1-R}$  are marked.

At the specimen EST05677-01-A, the axial load was raised very carefully in the first stage at 1.0 MPa confining pressure using some unloading-reloading cycles to detect initiation of dilatancy and to prevent sudden failure. After reaching the peak failure of about 29.4 MPa the axial load was reduced to about 10 MPa and then the confining pressure was increased to 2.3 MPa and subsequently, the axial load was increased again up to the next failure, the residual strength. The process was repeated at  $\sigma_3 = 4.3$  and 6.3 MPa with determination of the corresponding residual strengths.

The test on specimen EST05677-01-B was carried out more traditionally at a confining pressure of 3.3 MPa. The axial load was raised monotonically up to failure and then decreased beyond the failure and finally maintained constant at the residual strength of  $\sigma_{1-R} = 17$  MPa.

A complete multistage-process was performed on specimen EST05677-01-C. The confining pressure was elevated in three steps at 3.2, 7.4 and 15.8 MPa. In each of the last two steps the axial load was raised up to failure. After the last peak failure, the confining pressure was reduced in three steps from 15.8 MPa down to 7.4, 3.7 and 1.2 MPa at each of which the residual strength was obtained.

The last test with specimen EST05677-01-D was conducted only in two steps with determination of the peak strengths at confining pressures of 3.5 and 7.9 MPa, respectively.

All the specimens showed yield behaviour followed by strain hardening. The yield axial stress was determined between 16.5 and 19.0 MPa in the first confining stage at  $\sigma_3 = 1.0 - 3.5$  MPa. By further increasing the axial deformation dilatancy happened at higher deviatoric stresses beyond the yield ones.

To gain an insight into the volumetric change of the specimens determined by measuring the volume change of the expelled oil in the cell during the test, the volumetric strains in the first confining stage are illustrated separately in Figure 4-7 against axial stress for all the tests.

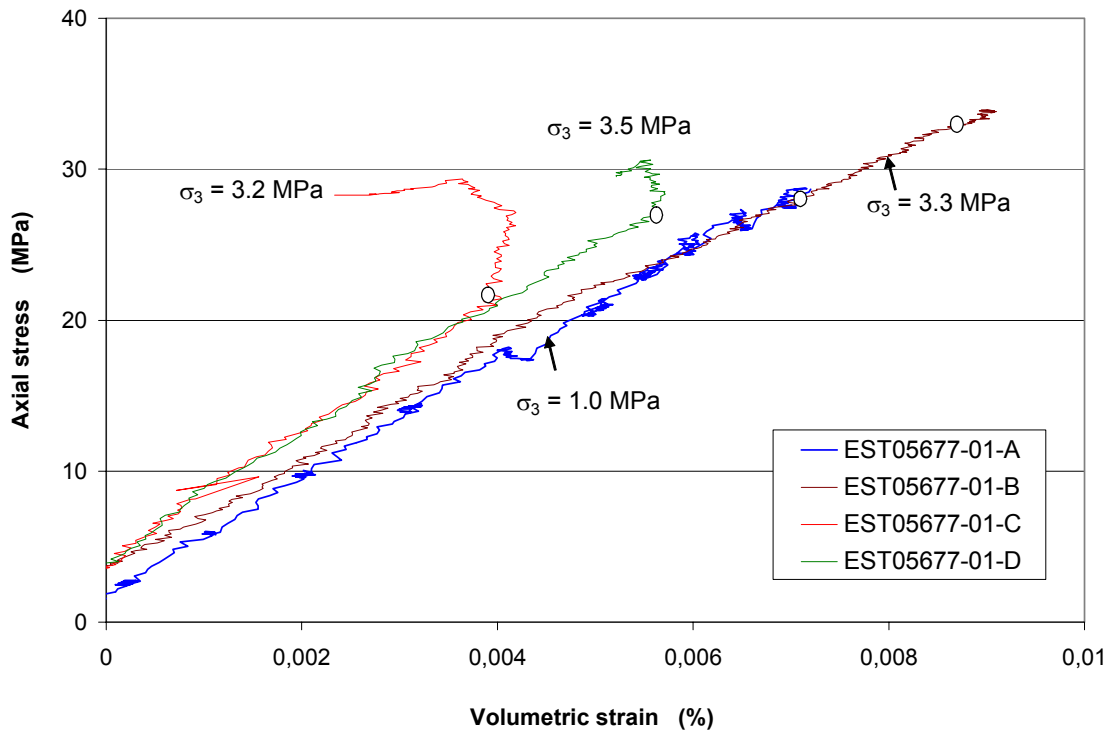


**Figure 4-7** Volumetric deformations of the specimens tested in the first confining stage

The specimens were compacted linearly with increasing the axial stress before the onset of dilatancy. The onset points of dilatancy are prior but near to failure. From the linear part of the curves of the volumetric strain  $\varepsilon_v$  versus the mean stress  $\sigma_m$  the elastic bulk modulus  $K = \Delta\sigma_m / \Delta\varepsilon_v$  was determined to range between 111.7 and 137.5 GPa, whereas Young's moduli measured on the linear part of the first loading curves are in the range of  $E = 3.1$  to  $3.5$  GPa. Based on these data and in accordance to  $K = E/3(1 - 2\nu)$ , Poisson's ratio was calculated at a constant value of  $\nu = 0.496$ . This indicates that the clay rock used in the tests (the specimens might be not fully saturated) is volumetrically incompressible in undrained conditions.

The specimens EST05677-01-A/B exhibited brittle failure at axial strains of 1.2 -1.3 % under confining pressures of 1.0 – 3.3 MPa. At the other two specimens EST05677-01-C/D, failure was not reached in the first confining stage, but the specimens were damaged. Further increasing the confining pressure led to specimen compaction which is indicated by higher slopes of the stress-strain curves in the subsequent higher confining stages. At confining pressures of 7.9 and 15.8 MPa, ductile deformations occurred before failure. The maximum deviatoric stresses obtained on the initially

undamaged specimens should represent the strength of the intact rock. The residual strength obtained at different confining pressures in the post-failure region should represent the strength of the rock mass with considerable discontinuities. All the characterisations determined in the multistage tests are summarised in Table 4.1.

**Table 4.1** Results of the multistage triaxial compression tests on specimens from the Callovo-Oxfordian argillites in zone B' at MHM-URL

Characteristic value in MPa	Specimen							
	EXT05677-01-A				EXT05677-01-B			
Confining pressure $\sigma_3$	1.0	2.3	4.3	6.3	3.3			
Yield stress $\sigma_{1-Y}$	16.5				17.0			
Initial dilatancy $\sigma_{1-D}$	28.0				33.0			
Peak strength $\sigma_{1-F}$	29.4				33.7			
Residual strength $\sigma_{1-R}$		15.4	21.8	27.7	17.0			
Young's modulus E (GPa)	3,3				3,5			
Bulk modulus $K^*$ (GPa)	130.0				111.7			
Poisson's ratio $\nu^*$ (-)	0.496				0.495			
	EXT05677-01-C						EXT05677-01-D	
Confining pressure $\sigma_3$	3.2	7.4	15.8	7.4	3.7	1.2	3.5	7.9
Yield stress $\sigma_{1-Y}$	18.0						19.0	
Initial dilatancy $\sigma_{1-D}$	21.3						27.0	
Peak strength $\sigma_{1-F}$		39.7	53.1				30.7	40.1
Residual strength $\sigma_{1-R}$			46.0	28.1	16.7	7.6		26.4
Young's modulus E (GPa)	3,1						3,4	
Bulk modulus $K^*$ (GPa)	137.5						137.5	
Poisson's ratio $\nu^*$ (-)	0.496						0.496	

$K^*$  and  $\nu^*$  were determined on basis of the measurements of the expelled oil volume as volumetric strain of the specimens.

In order to validate the method of multistage triaxial tests, the results of the peak strength and the residual strength obtained above are compared with the data obtained from the conventional triaxial tests performed by research partners of ANDRA on the specimens from the same rheological zone B' /SU 99/02/, as shown in Figure 4-8. It is obvious that the GRS-data are in a good agreement with ANDRA's data. Generally, peak and residual strength increase with confining pressure. Based on the GRS- and ANDRA-data, the strength parameters in the A) Hoek-Brown and B) Mohr-Coulomb failure criterion were estimated for the argillites in the zone B':

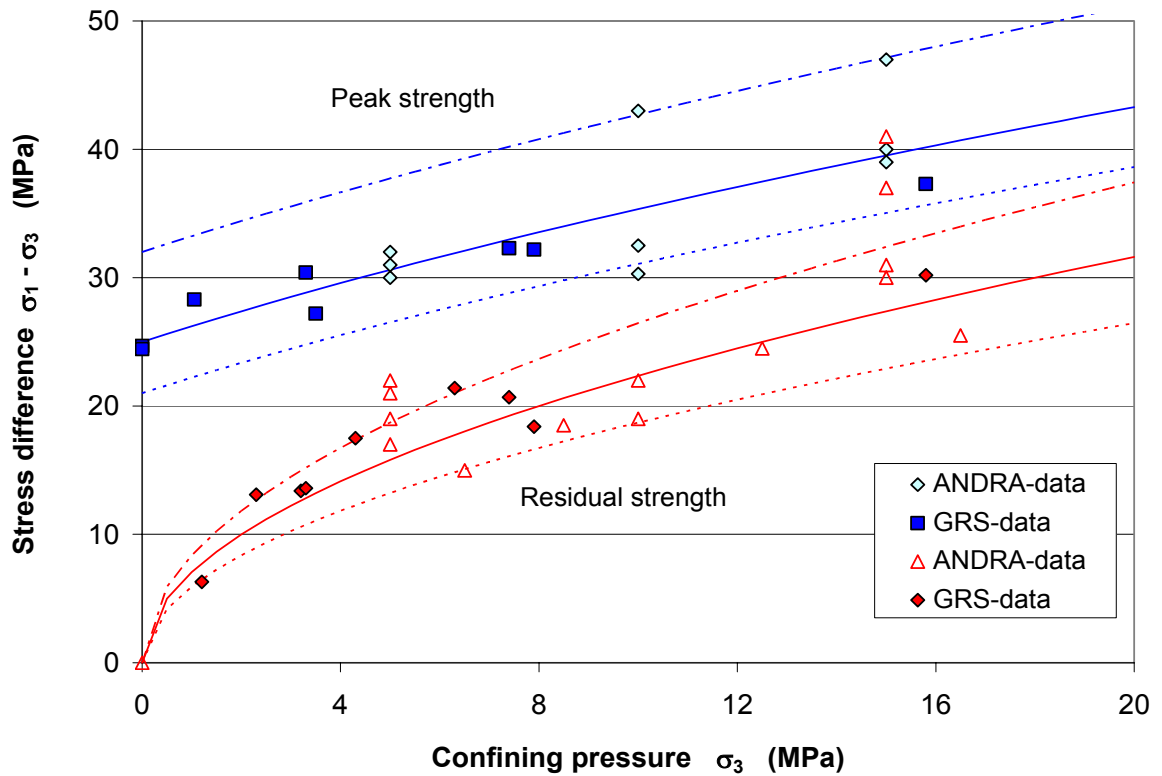


**Figure 4-8** Peak strength and residual strength of the Callovo-Oxfordian argillites at MHM-URL (zone B'), Hoek-Brown failure criterion

A) Hoek-Brown criterion: 
$$\sigma_1 = \sigma_3 + (m \cdot \sigma_c \cdot \sigma_3 + s \sigma_c^2)^{1/2} \quad (4.1)$$

where  $\sigma_c$  is the uniaxial compression strength,  $m$  and  $s$  are parameters. The parameter  $s$  depends on the fissuring conditions:  $s = 1$  for intact material and decreases toward to 0 with increasing fissures.

B) Mohr-Coulomb criterion: 
$$\tau = \sigma \cdot \tan \varphi + c \quad (4.2)$$

or 
$$\sigma_1 = 2 \cdot c \cdot \tan\left(45^\circ + \frac{\varphi}{2}\right) + \sigma_3 \tan^2\left(45^\circ + \frac{\varphi}{2}\right) \quad (4.2-1)$$

where  $\tau$  represents the soil shear strength,  $\sigma$  is the normal stress,  $c$  the cohesion and  $\varphi$  the friction angle.

The strength parameters are established for the average envelope and the low limit of the peak and the residual strength of the argillites in the zone B', as given in Table 4.2.

**Table 4.2** Strength parameters for the Callovo-Oxfordian argillites in zone B' at MHM-URL (based on the GRS-data and ANDRA-data)

Criterion	Mohr-Coulomb		Hoek-Brown		
	C (MPa)	$\varphi$ (°)	s (-)	m (-)	$\sigma_c$ (MPa)
Peak strength					
Mean envelope	9	19	1	2.5	25
Low limit	7.5	19	1	2.5	22
Residual strength					
Mean envelope	4.2	19	0	2.5	20
Low limit	3	19	0	2.5	14

The failure envelopes of the Hoek-Brown criterion with maximum and minimum limit are illustrated in Figure 4-8.

## **5 Long-term Mechanical Behaviour**

Knowledge of the long-term mechanical behaviour of host rocks is of most importance for long-term safety assessment of radioactive waste repositories. To characterise the long-term mechanical behaviour of the Callovo-Oxfordian argillites, creep and relaxation tests were performed by GRS.

### **5.1 Creep Behaviour**

#### **5.1.1 Testing Method**

Creep tests were carried out in creep rigs which allow to conduct long-term uniaxial creep tests simultaneously on up to five specimens with the same load. One rig was developed for creep tests on five specimens under ambient temperature and four other rigs allow two specimens to be tested in a chamber under elevated temperature up to 200°C. Figure 5-1 shows two rigs of them. Various specimen sizes of up to 100 mm in diameter and 250 mm length are acceptable. Axial load is applied to the specimens instantaneously and then maintained constant, controlled by means of an oil balance with an accuracy better than  $\pm 0.5$  % of readings. The maximum axial force is 500 kN. Specimen deformation is measured by displacement transducers (LVDT) with an accuracy better than  $\pm 0.2$  % of readings.

The testing plan took into account the following special aspects:

- All specimens were tested with the natural water contents. However, a very small loss of water from the specimens might occur during specimen preparation. Because of the high sensitivity of clays to moisture, it is necessary to prevent any moisture change of the specimens during the tests, especially during long-term creep tests. For this, all the specimens were sealed in rubber jackets and steel platens. Due to the very low permeability of the clay specimens an instantaneous loading may cause an immediate increase of the pore pressure. But it can disperse with time and tend to an equilibrium with interaction of the unconfined jacket in some days. In order to examine the influence of moisture change on the creep behaviour, two specimens were exposed to air in the testing room under constant load.



**Figure 5-1** Uniaxial testing machines for two and five simultaneous creep tests at GRS geotechnical laboratory in Braunschweig

- To study stress dependence of creep deformation from the limited specimen numbers, all the tests were carried out in multiple loading steps from very low level of 2 MPa to 15 MPa. Each elevation of the load was performed by applying an unloading-reloading cycle to examine reversible elastic and irreversible plastic deformation. Some results of the cycles have been presented in the form of stress-strain curves and Young's modulus in the section 4.2.

- To examine scale effects, two different specimen sizes were tested: six large specimens with 100 mm diameter and 200 mm length, and five small ones with 45 mm diameter and 90 mm length. It should be noted here that large specimens can generally provide more realistic data for characterising the rock mass and also allows an higher accuracy of the applied stress due to the relative larger specimen cross section loaded under a certain force fluctuation.
- To observe the effect of material anisotropy on the creep behaviour, two small specimens were loaded in the direction perpendicular to the bedding plane and three parallel to the bedding. All the large specimens were loaded perpendicular to the bedding.
- Finally, each creep test duration must be long enough to gain sufficient confirmed creep data, especially of the creep rate because the usual limit of strain rate resolution of the rigs is about  $\dot{\epsilon} = 10^{-10} \text{ s}^{-1}$  for creep durations of days up to weeks. In the tests, the duration of each creep phase varied from about one to seven months.

In accordance with the loading conditions, the creep tests were divided into four groups, each of them consisting of two or five specimens loaded in the same rig. The loading conditions and the creep durations of all the tests are summarised in Table 5-1.

### 5.1.2 Results

Results of the creep tests are shown in Figure 5.2 for Group I, Figure 5-3 for Group II, Figure 5-4 for Group III and Figure 5-5 for Group IV, respectively. Because load and temperature are the most important parameters for the interpretation of the results, their measuring results are plotted versus time for each group. The development of axial strain versus time and creep rate as a function of strain are illustrated for each specimen.

- Group I

The two large specimens EST05582-01-II and EST05630-01-II with D/L = 100 mm /200 mm were loaded in the direction perpendicular to the bedding plane in four creep

**Table 5.1** Overview of the uniaxial creep tests on the specimens from the Callovo-Oxfordian argillites at MHM-URL

Test-group	Specimen	Depth (m)	Size D/L (mm)	Bulk density (g/cm <sup>3</sup> )	Water content* (%)
I	EST05582-01	463.4	100/200	2.392	8.7
	EST05630-01	474.2	100/200	2.378	8.9
II	EST05481-01	434.6	100/200	2.457	
	EST05671-01	484.2	100/180	2.448	7.4
III	EST05677-01	487.1	100/200	2.405	7.1
	EST05751-01	505.7	100/200	2.444	6.4
IV	EST05582-02	463.2	45/90	2.405	8.7
	EST05582-03	463.2	45/90	2.404	8.7
	EST05630-02	474.1	45/90	2.384	8.9
	EST05671-02	484.1	45/90	2.437	7.4
	EST05671-03	484.1	45/90	2.438	7.4

Axial load  $\sigma_1$  (MPa) and creep duration  $\Delta t$  (day) in each creep step

Specimen	Step	1.	2.	3.	4.	5.	6.
	Direction	$\sigma_1/\Delta t$	$\sigma_1/\Delta t$				
EST05582-01	II	2.0/21	4.95/54	7.95/96	11.9/22		
EST05630-01	II	2.0/21	4.95/54	7.95/96	11.9/22		
EST05481-01	II	3.0/21	6.0/54	9.9/96	11.9/76	9.9/74	11.9/46
EST05671-01	II	3.0/21	6.0/54	9.9/96	11.9/76	9.9/74	11.9/46
EST05677-01	II	2.0/21	4.95/90				
EST05751-01	II	2.0/21	4.95/90				
EST05582-02	II	5.0/21	8.0/54	12.0/96	15.0/76	15./124/ desaturation	
EST05582-03	II	5.0/21	8.0/54	12.0/96	15./200		
EST05630-02	=	5.0/21	8.0/54	12.0/96	15.0/76	15./124/ desaturation	
EST05671-02	=	5.0/21	8.0/54	12.0/96	15./200		
EST05671-03	=	5.0/21	8.0/54	12.0/96	15./200		

II : Load direction perpendicular to the bedding plane; =: Load direction parallel to the bedding plane. \*: The values of water content correspond to the saturated states, slightly higher than the true water contents of the tested specimens

steps. Figure 5-2 A shows that the temperature and the axial loads were quite constant during each creep step. Temperature was kept at 23°C in the first creep phase and at 24°C in the others with a fluctuation of  $\pm 0.1^\circ\text{C}$ , whereas the accuracy of the applied stresses is better than 1 % of readings. From the creep curves shown in Figure 5-2 B, it is obvious that the clay rock creeps even under a very low stress of 2 MPa. This observation indicates that there exists no lower creep limit below which no creep occurs. Transient creep occurred after each sudden reloading. To examine whether steady state creep was reached, the creep rates were determined from the strain increments in various time intervals from a half day to 20 days. Figure 5-2 C gives the creep rates as a function of axial strain for each creep step. It is clearly to be seen that the creep rate decreases with increase of the strain. In the first two creep phases at 2.0 and 4.95 MPa any constant creep rates were not reached. After about 70 days creeping of the third phase at 7.95 MPa, the creep of both specimens seemed to reach steady states. The steady state creep strain ranges to about 0.06 %, corresponding to 30 % of the total creep strain of 0.19 %. The steady state creep rates were determined to:  $\dot{\epsilon} = 1.34 \cdot 10^{-10} \text{ s}^{-1}$  for EST05630-01 and  $\dot{\epsilon} = 9.20 \cdot 10^{-10} \text{ s}^{-1}$  for EST05582-01, as shown more clearly in Figure 5-2 D. The last creep phase at 11.9 MPa lasted for about 22 days and then broke down as the rig failed. In this creep phase only transient creep occurred.

- Group II

The two large specimens EST05481-01-II and EST05671-01-II with D/L = 100 mm / 200 mm were loaded in the direction perpendicular to the bedding plane in six creep steps, but the data of the first two steps of the specimen EST05671-01 are unavailable due to difficulties with the data acquisition. Figure 5-3 A shows the temperature and the axial loads versus time, while Figure 5-3 B gives the creep curves and Figure 5-3 C-D the creep rates as a function of the axial strain. In this group of the tests, a stress drop process was performed after the fourth creep phase from the load of 11.9 MPa down to 9.9 MPa for 74 days. After the stress drop the specimens deformed backward with negative strain rates for several days. Due to recovery, the creep returned forward again. From the creep rate data of specimen EST05481-01 shown in Figure 5-3 C, one can see that the steady state was reached at 9.9 MPa not only in the third phase but also in the reduced stress phase. The steady state creep rates determined in the both phases are in a good agreement with an average value of  $\dot{\epsilon} = 4.3 \cdot 10^{-11} \text{ s}^{-1}$ . This should support the existence of steady state creep conditions for the Callovo-Oxfordian

argillites. At specimen EST05671-01 a steady state was not reached in the third phase at 9.9 MPa, but in the reduced stress phase with a creep rate of  $\dot{\epsilon} = 6.0 \cdot 10^{-11} \text{ s}^{-1}$  at 9.9 MPa (Figure 5-3 D). During the reduced stress phase, the temperature controller failed for 3 days, lowering the temperature down from 24°C to 18.5°C, and then staying constant at 22.5°C (Figure 5-3 A). This temperature change resulted in slight backward deformations for both specimens (Figure 5-3 B). After the reduced stress phase, the specimens were reloaded to the same level of 11.9 MPa as before. The creep of the each specimen in the last phase reached a steady state after a relatively short period of transient creep. Under the same load of 11.9 MPa, but at different temperatures of 24°C in the fourth phase and 22.5°C in the last phase, different steady state creep rates were obtained, as shown in Figures 5-3 C-D.

- Group III

In this group of the tests, the first two creep phases of Group I at 2.0 and 4.95 MPa were repeated using the specimens EST05677-01 and EST05751-01 to examine the location dependence of the creep behaviour of the argillites. The testing conditions and results are given in Figure 5-4 A-C. Over the transient creep phase at 4.95 MPa, quasi-steady states were reached for both specimens with rates of  $\dot{\epsilon} = 1.51 \cdot 10^{-10} \text{ s}^{-1}$  for EST05751-01 and  $\dot{\epsilon} = 1.75 \cdot 10^{-10} \text{ s}^{-1}$  for EST05677-01. After the creep tests both deformed specimens were used for the triaxial tests (see section 4.2), but only on four small specimens from sample EST05677-01. Figure 5-4 D gives a comparison of the creep curves obtained under the same conditions for the four specimens from different depths between about 463 and 506 m. It can be seen that the deformations and also the creep rates decrease slightly with increasing depth.

- Group IV

Five small specimens with 45 mm diameter and 90 mm length were tested simultaneously at room temperature in four creep steps. Two specimens EST05582-02-II and EST05582-03-II were loaded in the direction perpendicular to the bedding plane, while the other three of EST05630-02-=-, EST05671-02-=-, and EST05671-03-=- parallel to the bedding. From Figure 5-5 A one can see that the fluctuations  $\Delta\sigma = \pm 0.2$  MPa of the applied stresses and  $\Delta T = \pm 1^\circ\text{C}$  of the temperature are larger than in the other tests using the large specimens placed in the chambers.

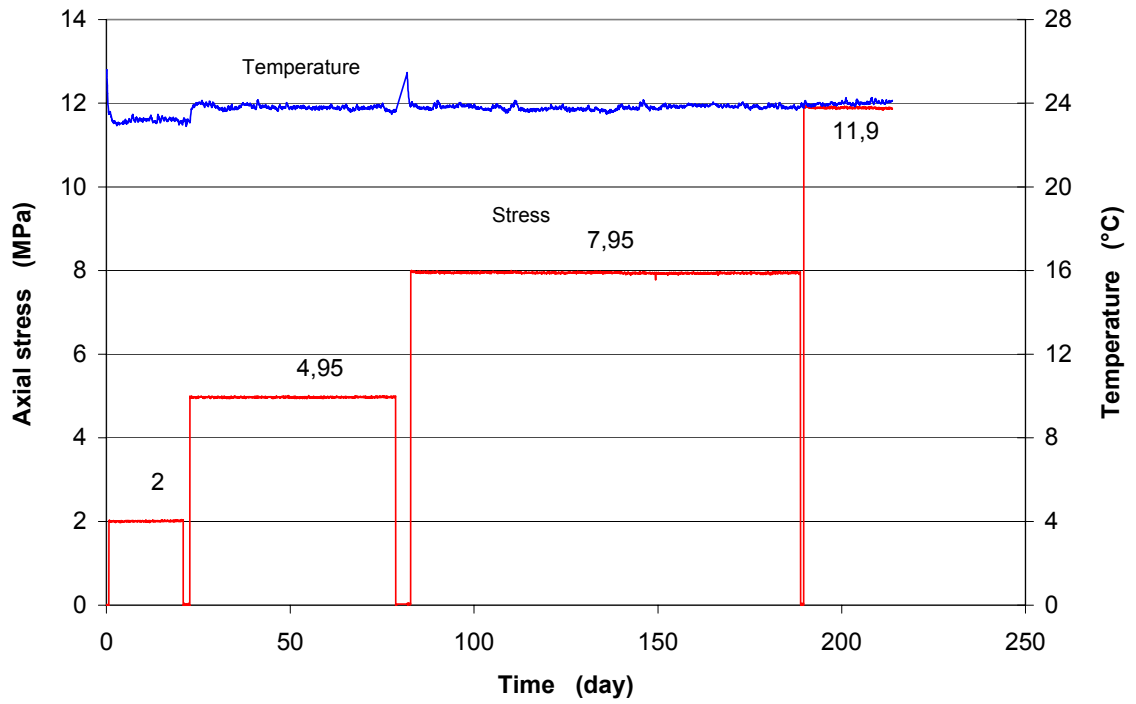


Figure 5-2 A Temperature and axial stress versus time

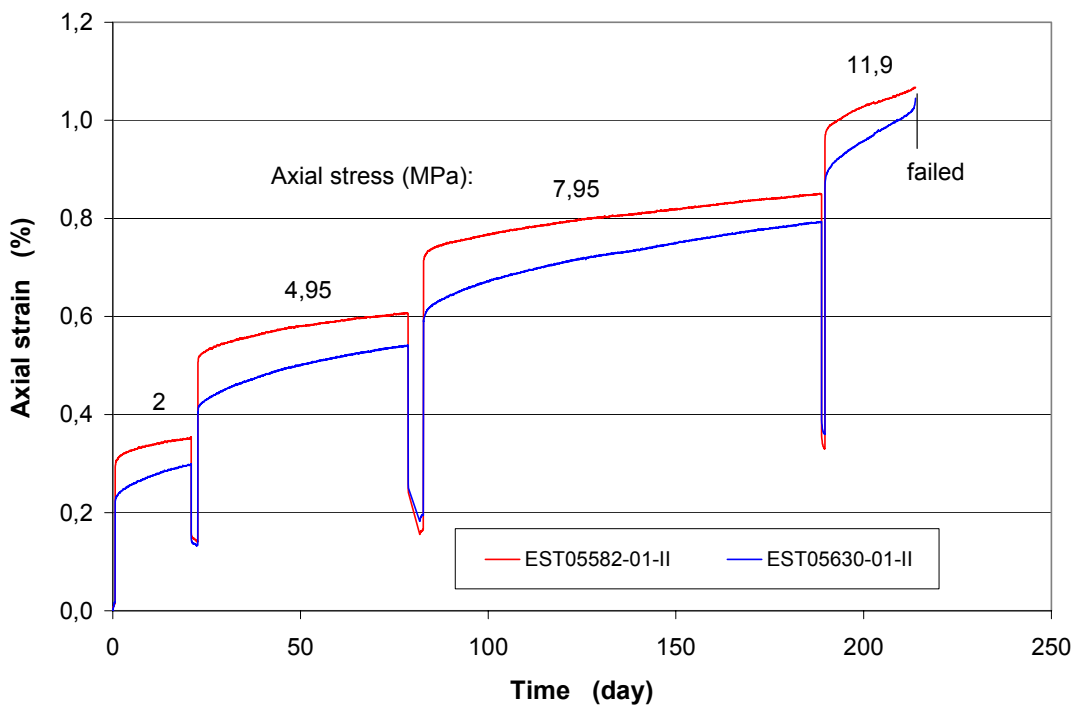


Figure 5-2 B Axial strain versus time

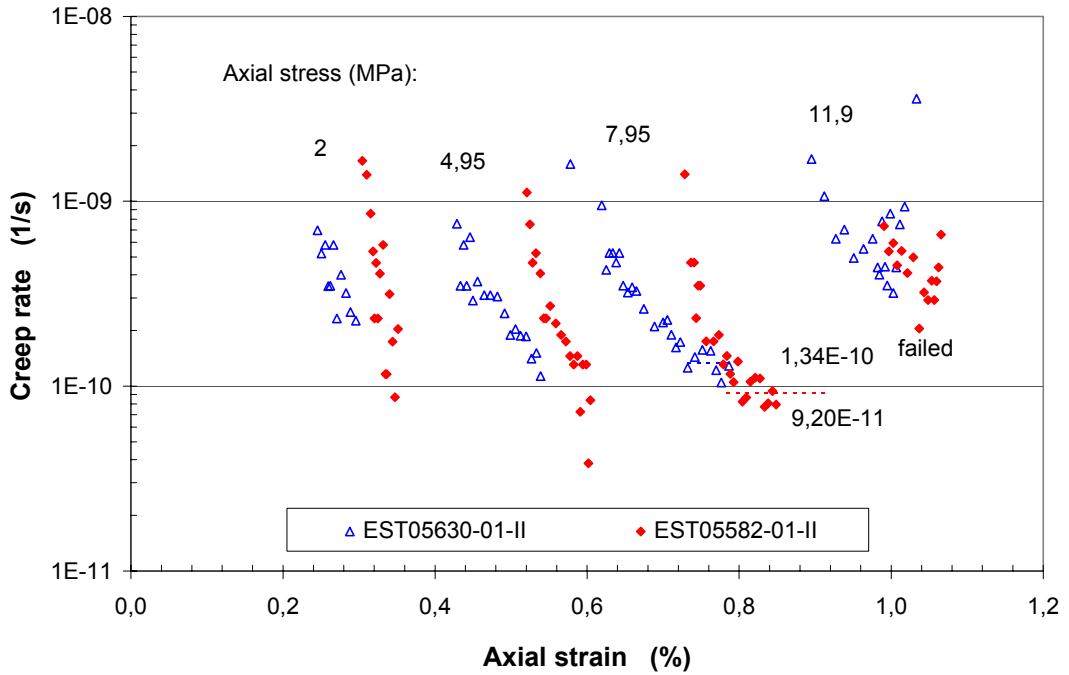


Figure 5-2 C Creep rate versus axial strain

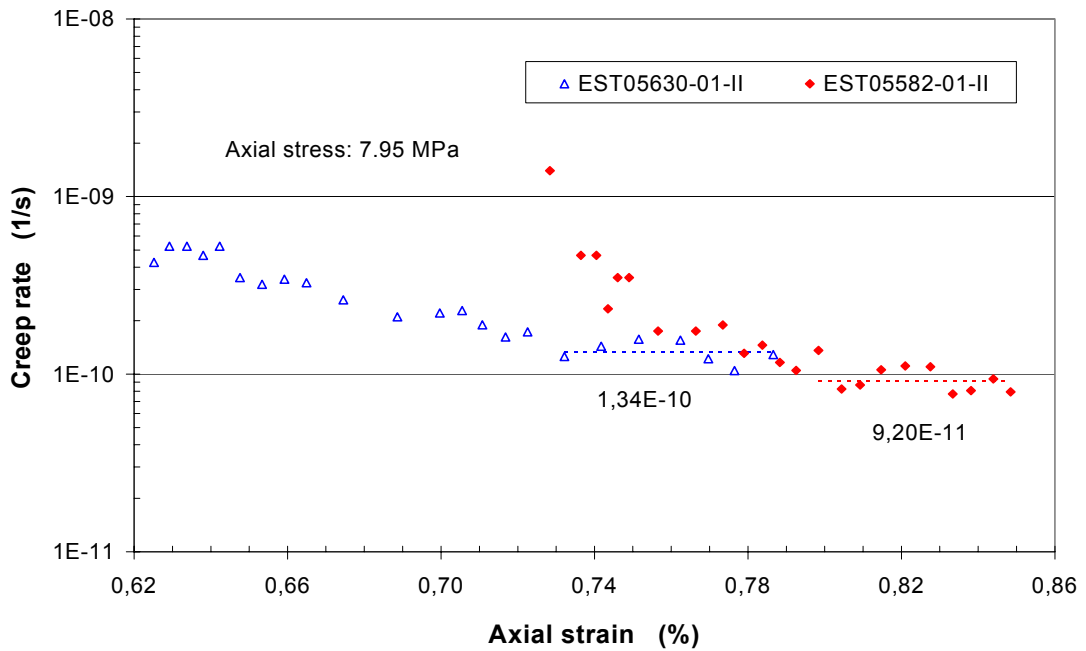


Figure 5-2 D Steady state creep rate at load step 7.95 MPa

Figure 5-2 Group I: Two simultaneous uniaxial creep tests on the specimens EST05582-01 and EST05630-01 at ambient temperature with four succeeding stresses

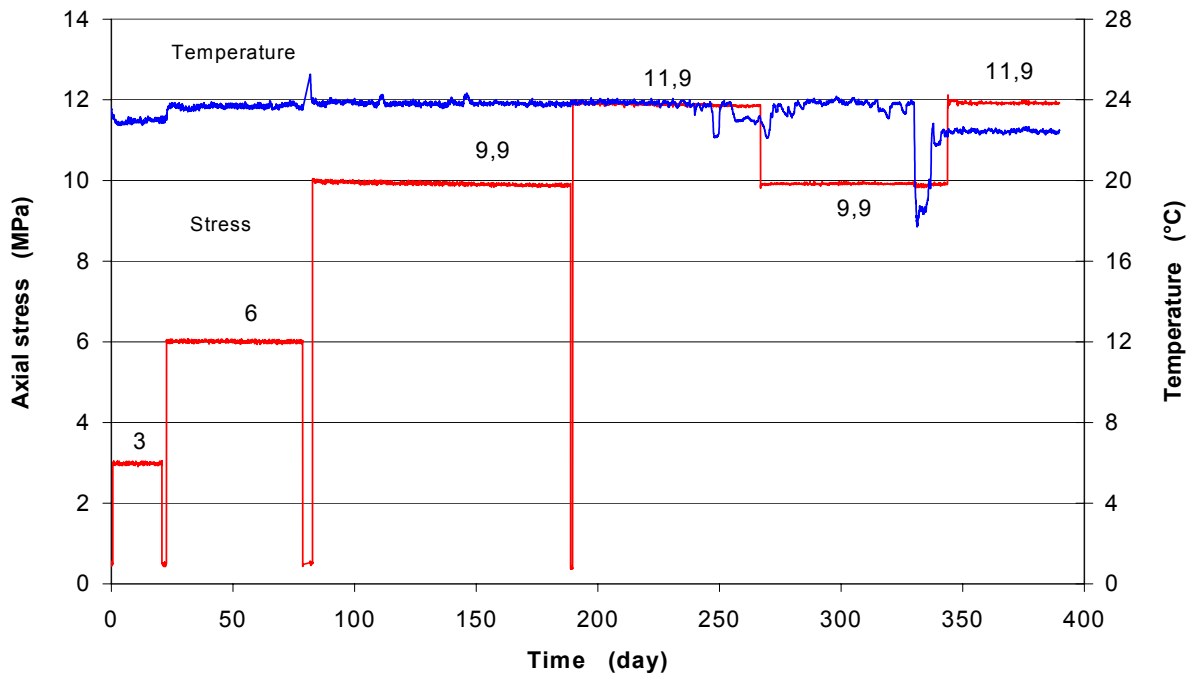


Figure 5-3 A Temperature and axial stress versus time

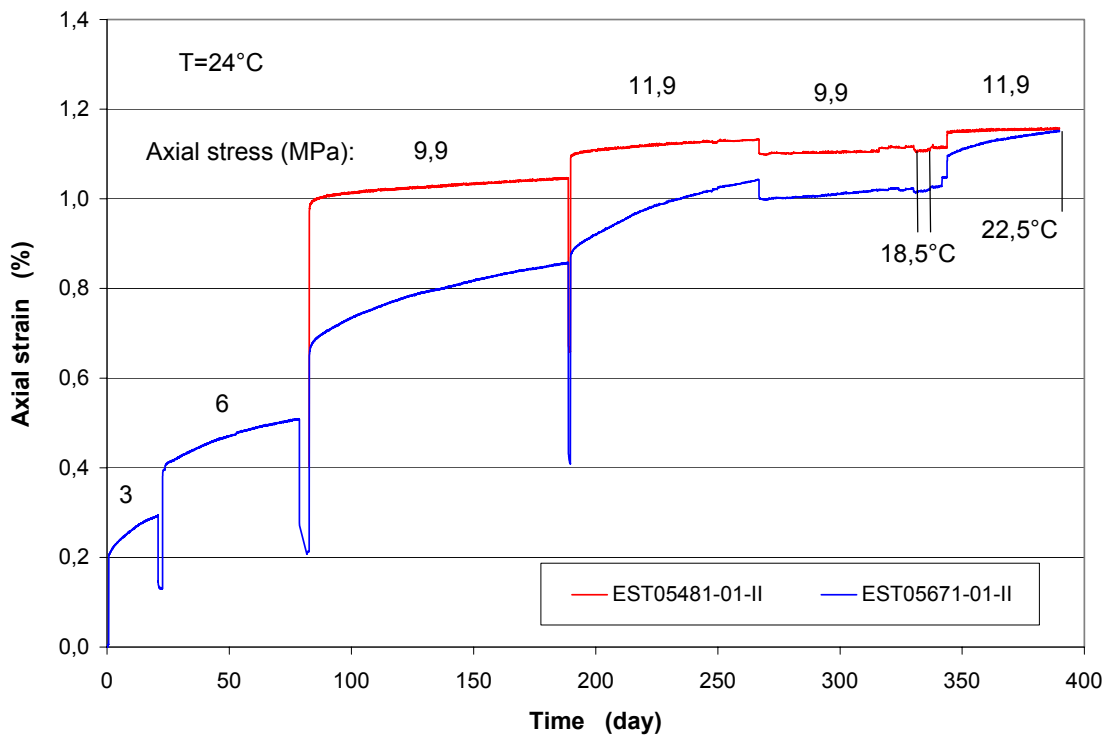
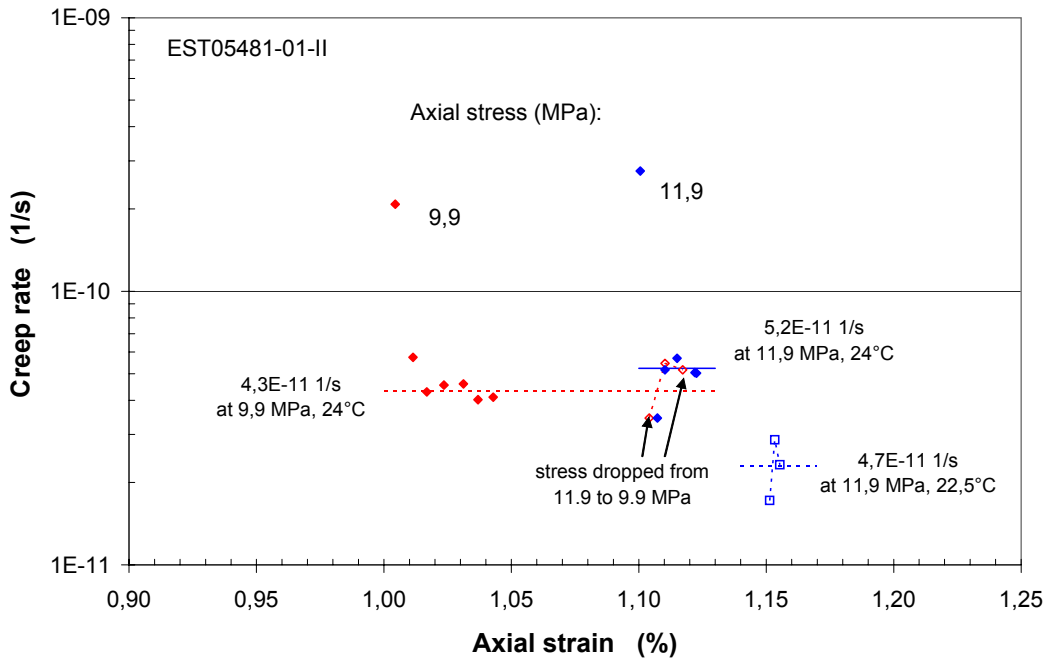
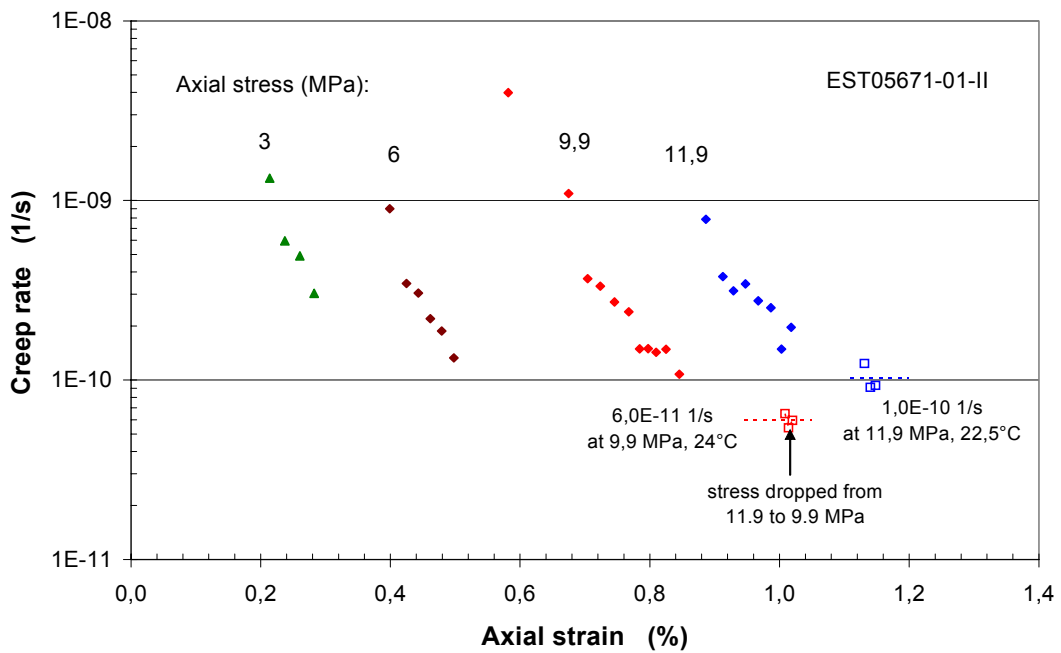


Figure 5-3 B Axial strain versus time



**Figure 5-3 C** Creep rate versus axial strain, specimen EST05481-01



**Figure 5-3 D** Creep rate versus axial strain, specimen EST05671-01

**Figure 5-3** Group II: Two simultaneous uniaxial creep tests on the specimens EST05481-01 and EST05671-01 at ambient temperature with six succeeding stresses

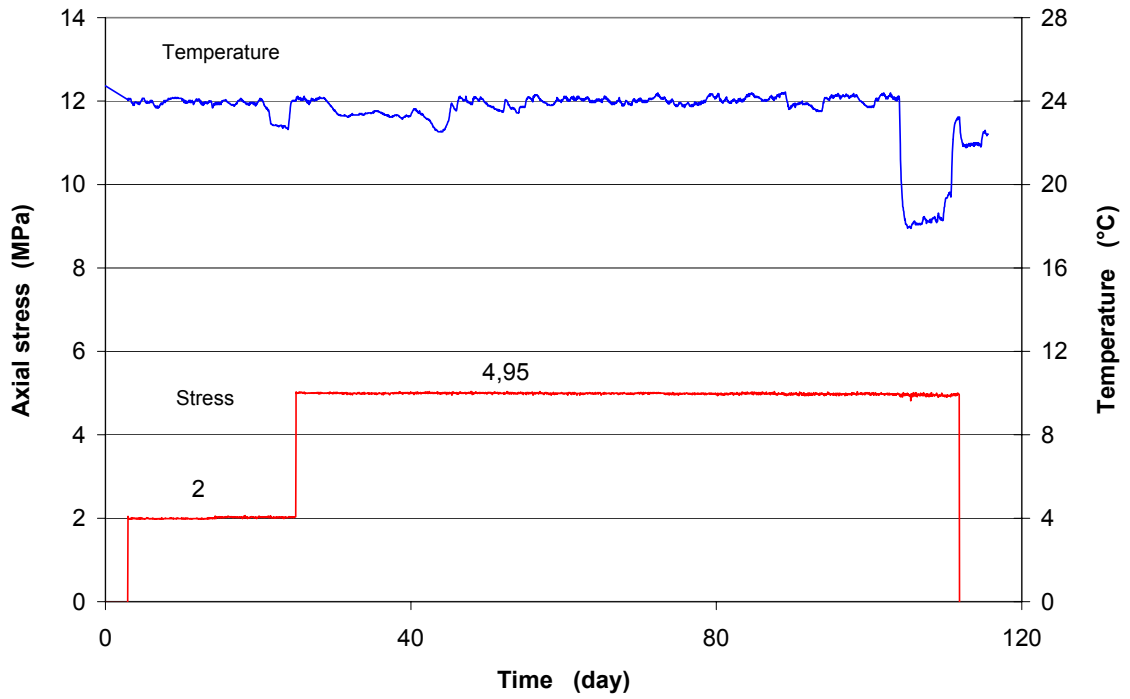


**Figure 5-4 A** Temperature and axial stress versus time

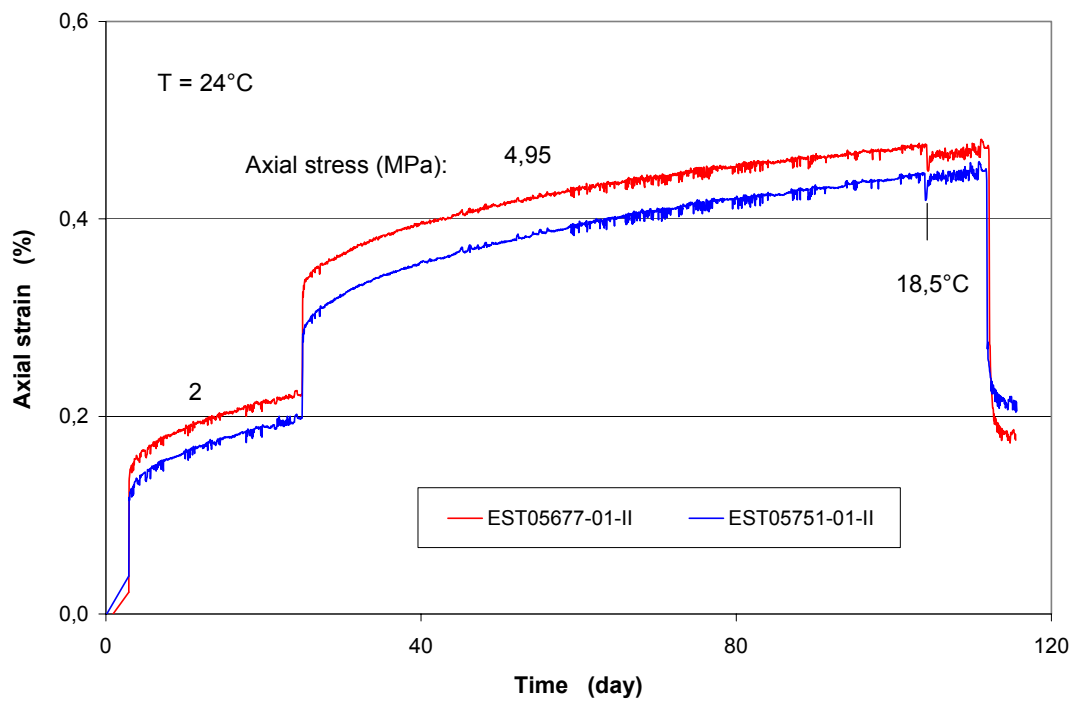


**Figure 5-4 B** Axial strain versus time

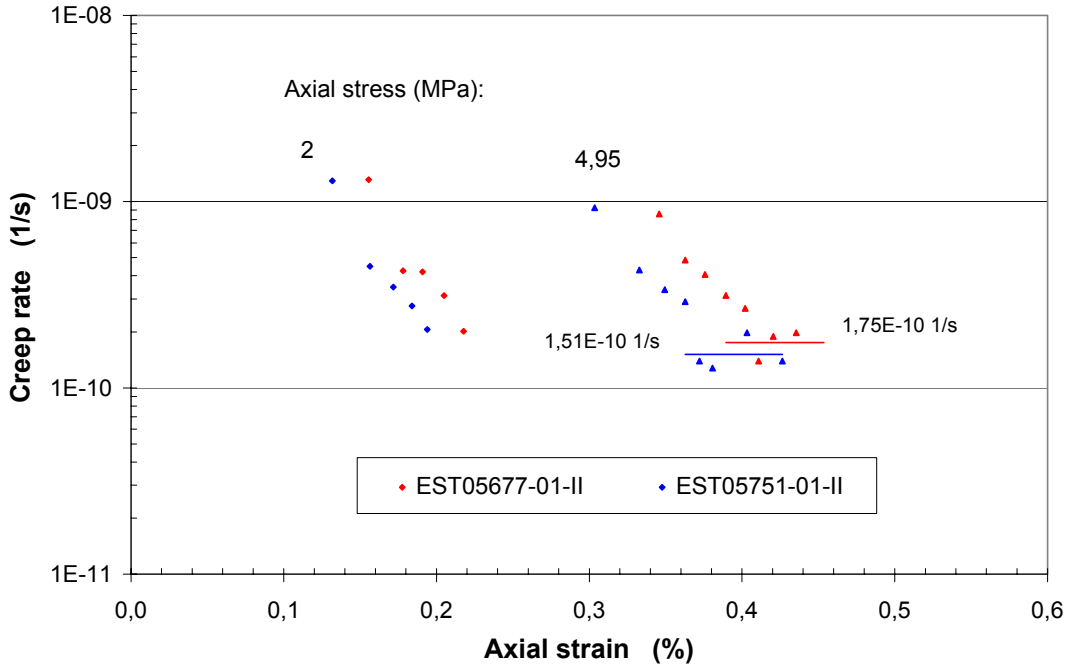


**Figure 5-4 C** Creep rate versus axial strain

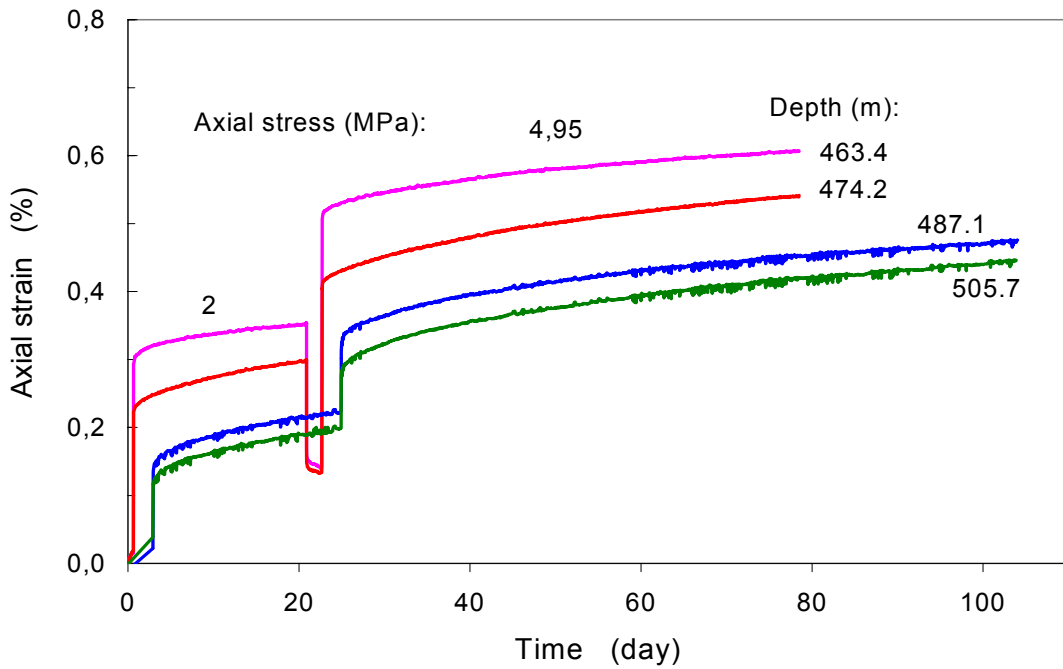


**Figure 5-4 D** Location dependence of the creep behaviour

**Figure 5-4** Group III: Two simultaneous uniaxial creep tests on the specimens EST05677-01 and EST05751-01 at ambient temperature with two succeeding stresses

By comparing the creep curves shown in Figure 5-5 B-C, it can be found that the total deformations in the direction perpendicular to the bedding are larger than parallel to the bedding and the creep in the direction perpendicular to the bedding is slightly faster than parallel to the bedding. For instance, the average quasi-steady state creep rate of  $\dot{\epsilon} = 1.7 \cdot 10^{-10} \text{ s}^{-1}$  perpendicular to the bedding is on average about 1.4 times higher than  $\dot{\epsilon} = 1.2 \cdot 10^{-10} \text{ s}^{-1}$  parallel to the bedding, determined at the stress of 12 MPa. The same conclusion can also be drawn from the creep rate data obtained at 15 MPa. Generally, the anisotropy effect on the creep behaviour of the clay rock is not significant in comparison with the other factors such as mineralogical composition and water content.

In the last creep phase at 15 MPa, two specimens were exposed to the room air with relative humidity of  $24.0 \pm 3.4 \%$  in order to examine the effect of moisture on the creep behaviour, as shown in Figure 5-5 C. Because a direct measurement of the desaturation of the creeping specimens was impossible, an accompanying measurement of water content change of a 250g specimen was conducted under the same conditions as in the creep tests (Figure 5-5 C). As the specimens were rapidly desaturated during the first days, the deformations responded simultaneously with a large magnitude of about 0.3 % shrinkage, independent of the loading direction. The fluctuations of the deformations corresponded to the moisture fluctuations. After sealing the specimens against the air conditions in the room, the fluctuations of the deformations were minimised. Over the last 40 days, under the stress of 15 MPa, the air-dried specimens deformed steadily backward with negative rates of  $-10^{-11} \text{ s}^{-1}$  (swelling). The desaturation effect on the creep behaviour was also observed in the hydrostatic compression tests at pressures of 5 and 15 MPa by Gasc-Barbier et al. /GAS 00/, using specimens from the argillaceous formation Callovo-Oxfordian, too.

Figure 5-6 shows a comparison between the creep curves of the large and small specimens, three of which were taken from the same core EST05582. It can be seen that at the same stresses, the total strains of the large specimens are higher than those of the small ones. However, the pure creep strains and the creep rates are quite similar. This means, there exists a scale effect only on the short-term behaviour of the clay rock, but the scale effect on its creep behaviour is negligible.

To examine the stress dependence of the creep rate, the quasi - steady state creep rates obtained above are illustrated in Figure 5-7 as a function of the applied stresses.

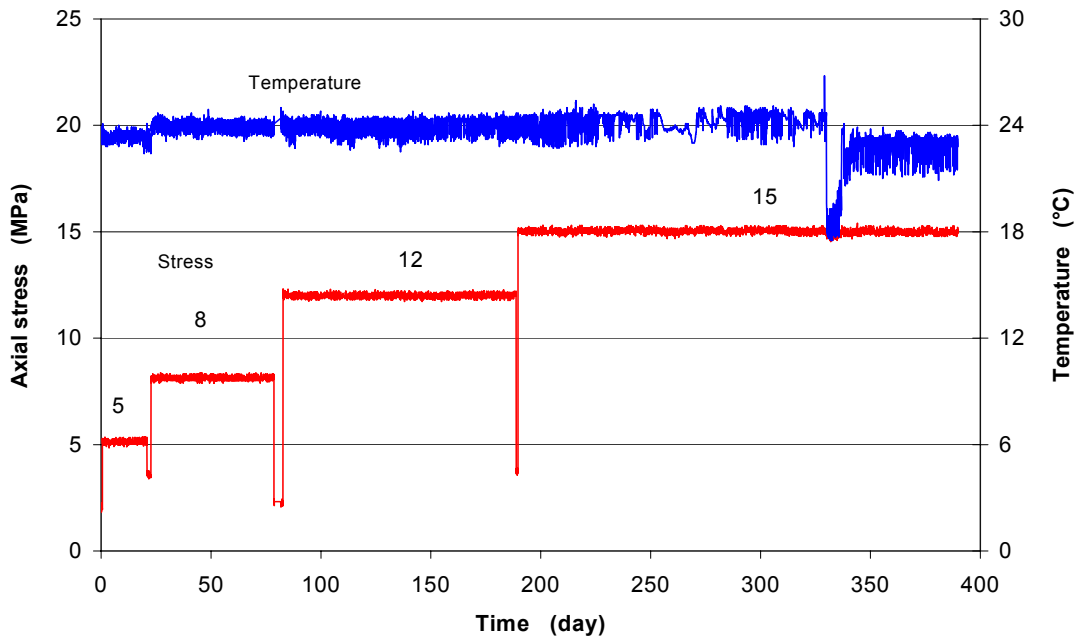


Figure 5-5 A Temperature and axial stress versus time

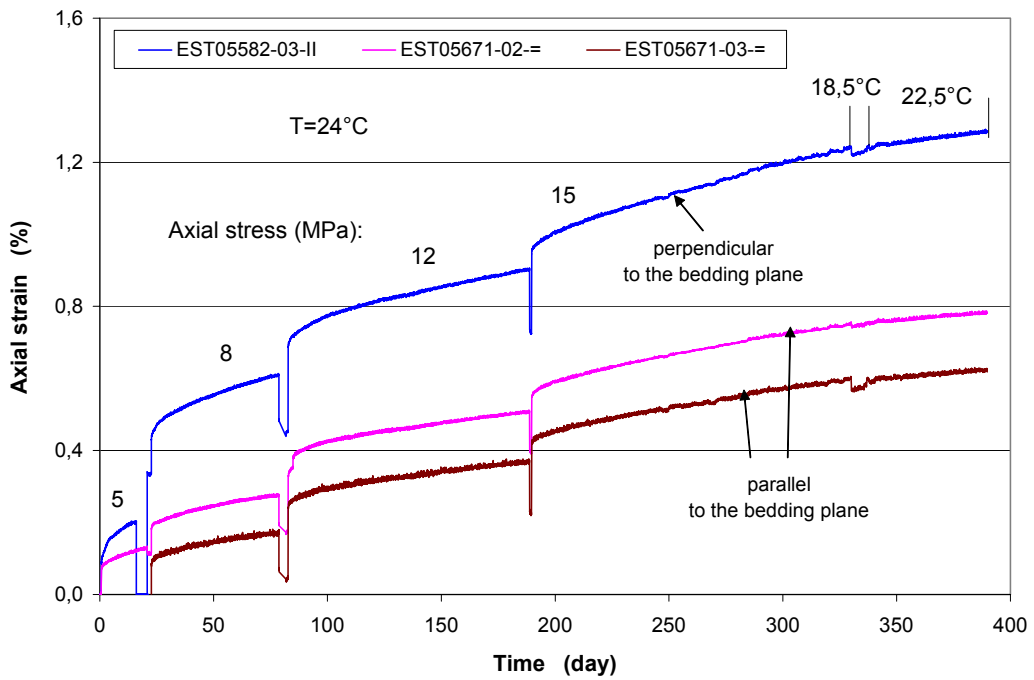


Figure 5-5 B Axial strain versus time

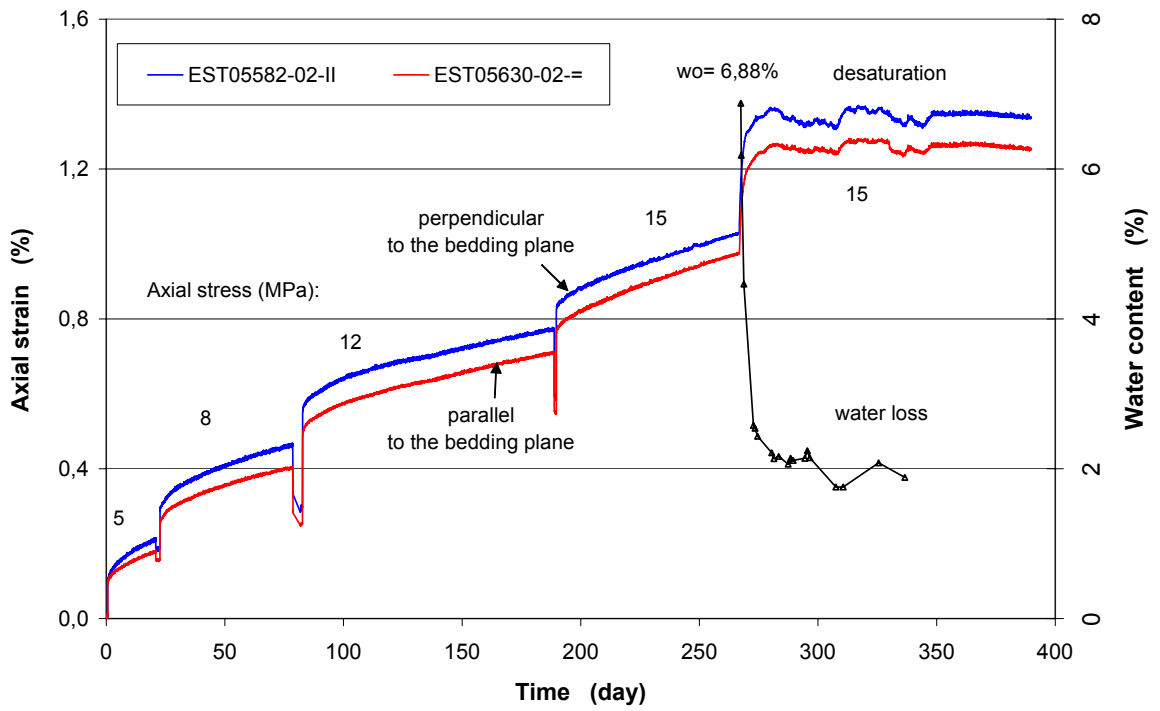


Figure 5-5 C Axial strain versus time and desaturation

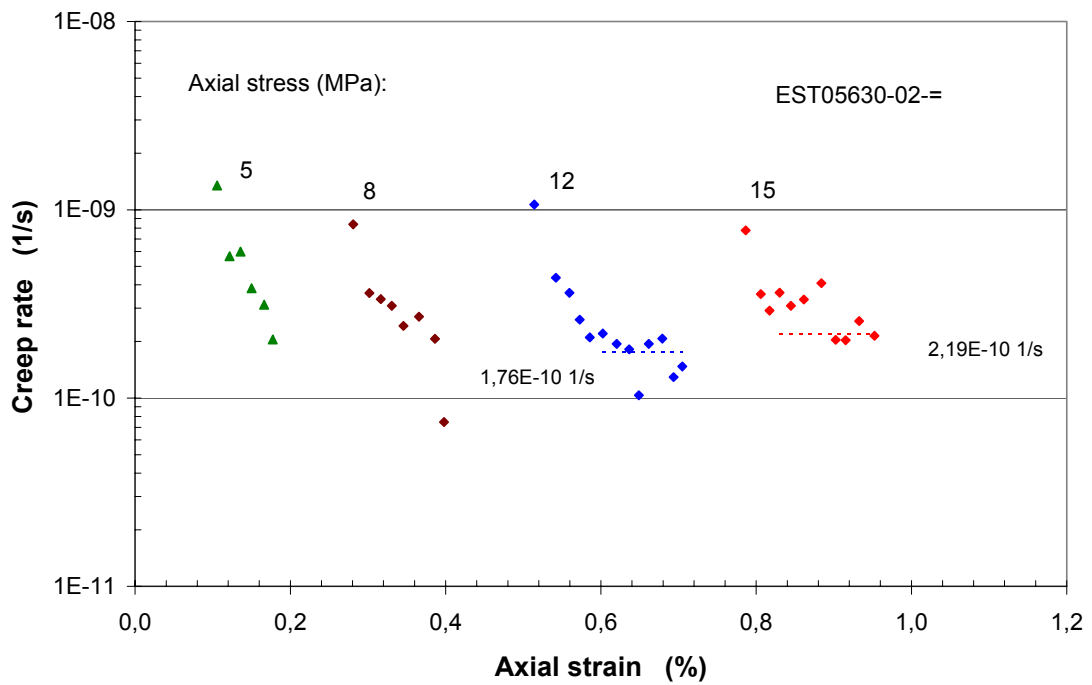


Figure 5-5 D Creep rate versus axial strain, specimen EST05630-02

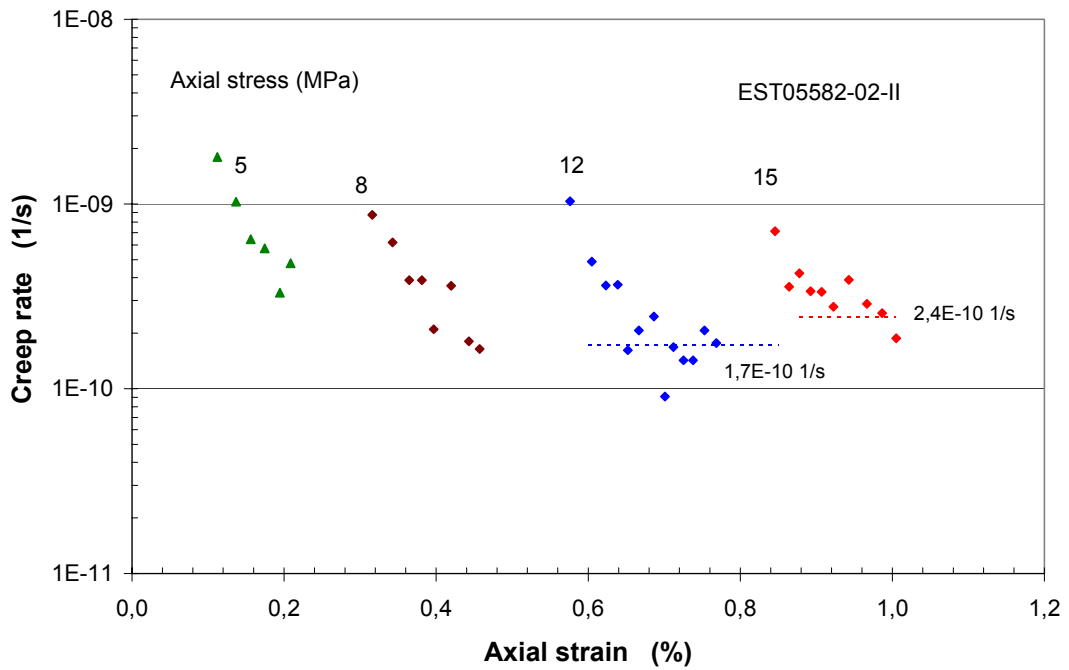


Figure 5-5 E Creep rate versus axial strain, specimen EST05582-02

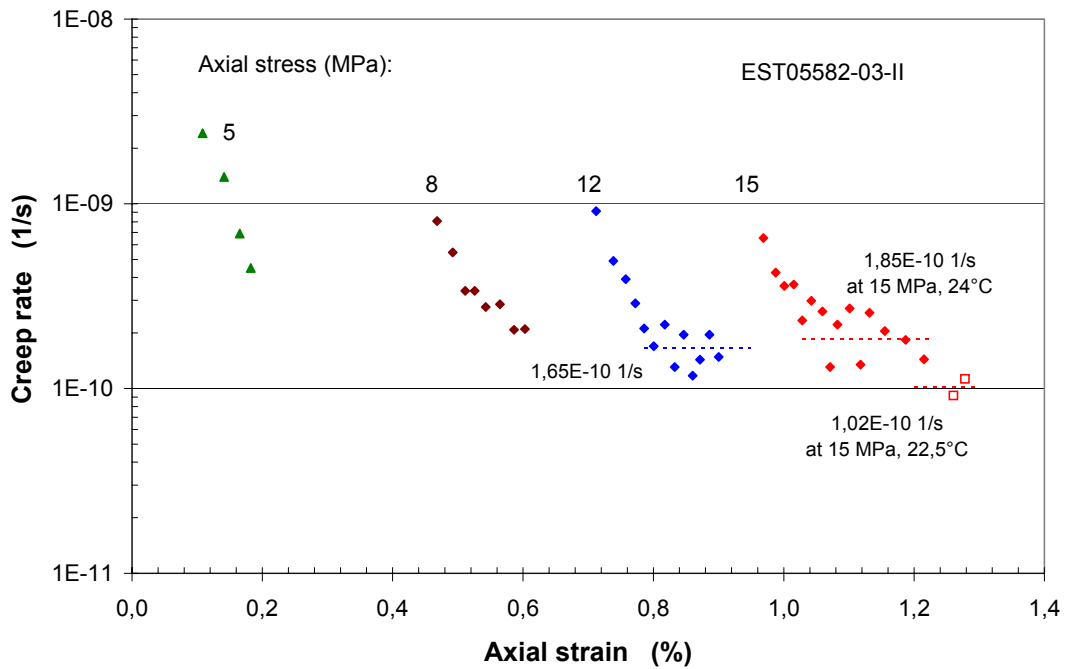


Figure 5-5 F Creep rate versus axial strain, specimen EST05582-03

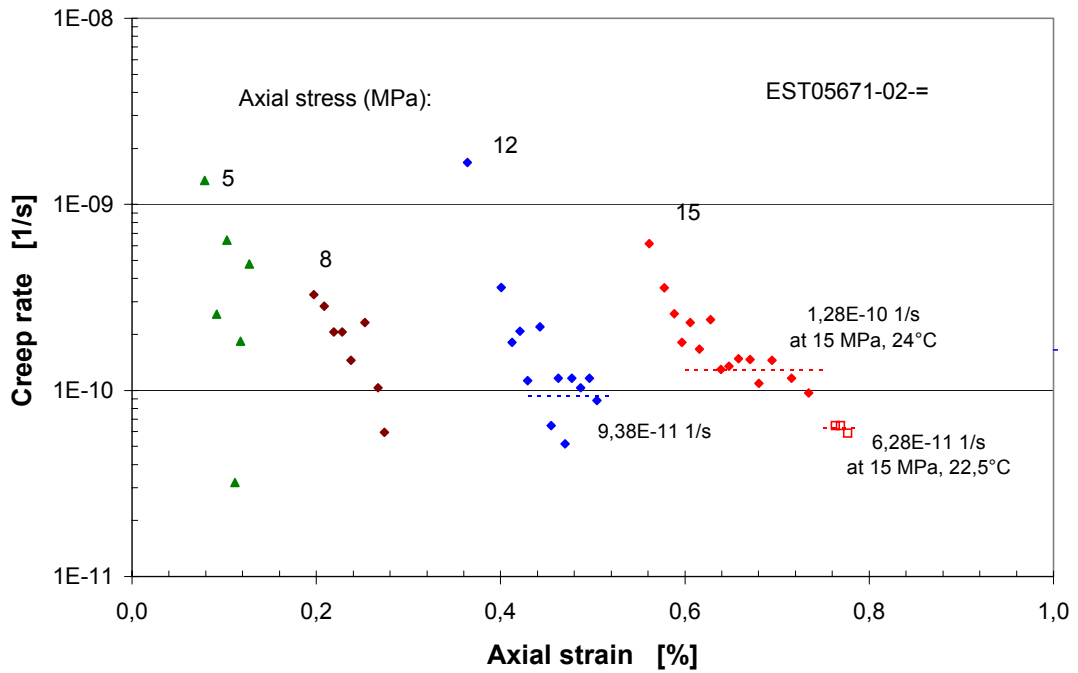


Figure 5-5 G Creep rate versus axial strain, specimen EST05671-02

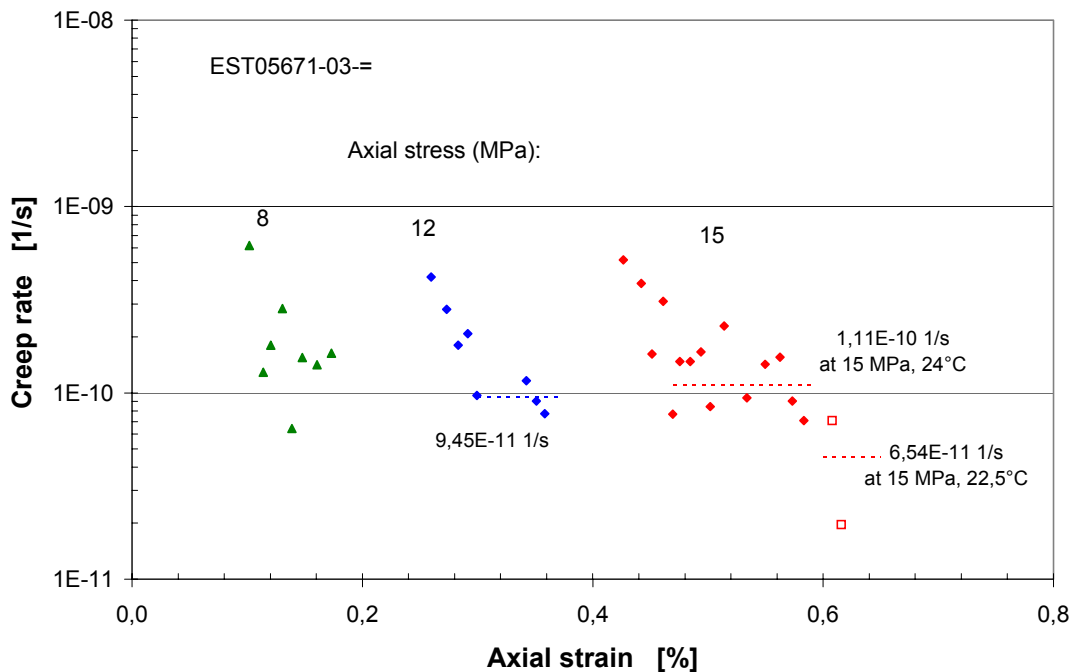


Figure 5-5 H Creep rate versus axial strain, specimen EST05671-03

Figure 5-5 Group IV: Five simultaneous uniaxial creep tests on the specimens EST05630-02, EST05582-02, EST05582-03, EST05671-02 and EST05671-03 at ambient temperature with four succeeding stresses

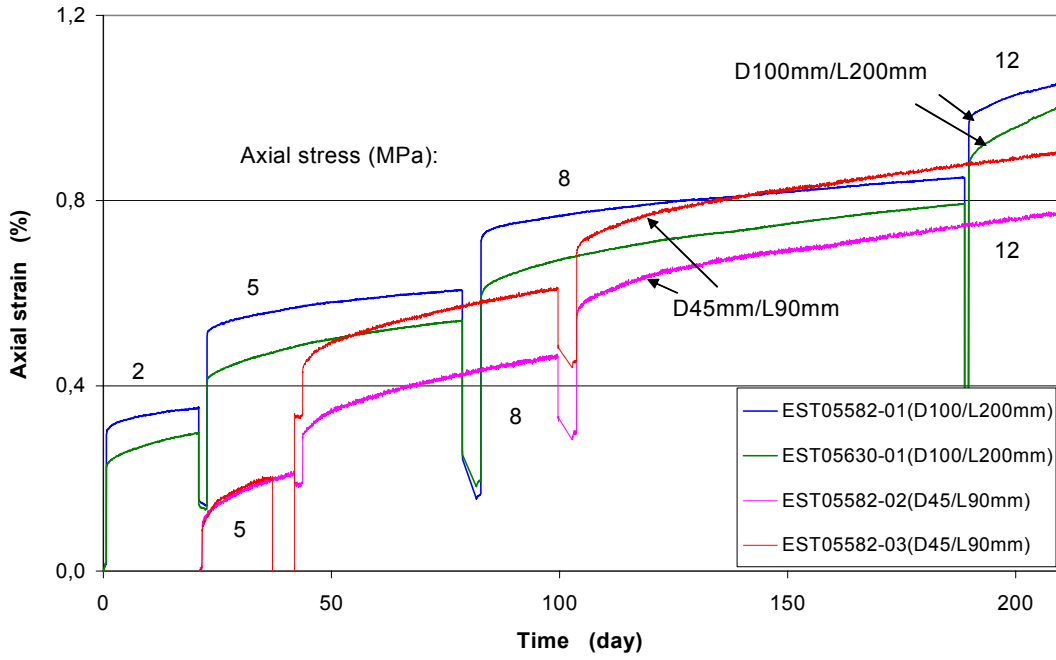


Figure 5-6 Scale effect on the creep behaviour

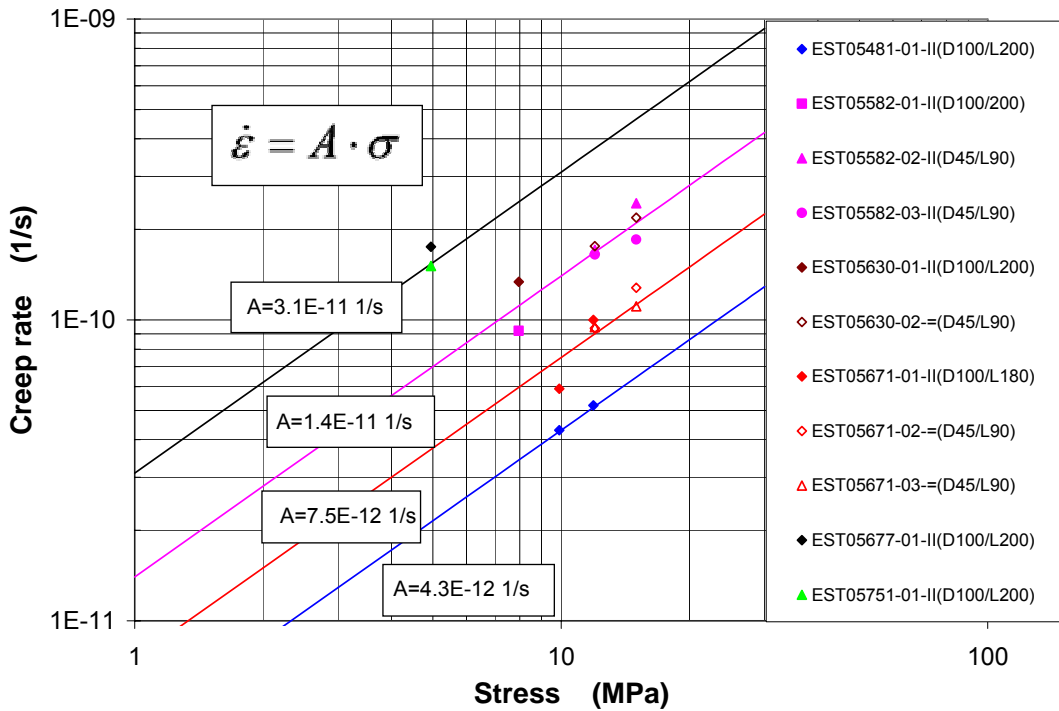


Figure 5-7 Quasi - steady state creep rates as a function of the applied stresses determined on specimens from the Callovo-Oxfordian argillites at ambient temperature

It can be recognised that the rates differ by a factor of less than 7 from one specimen to another. Most interesting is that a linear relationship of the quasi - steady state creep rate to the stress can be deduced for each specimen (or location) respectively, if the negligible effects of the specimen size and the creep direction are unconsidered. The general form is:

$$\dot{\varepsilon} = A \cdot \sigma \quad (5.1)$$

where  $\dot{\varepsilon}$  is the quasi - steady state creep rate,  $\sigma$  is the applied stress, and A is a parameter which is a function of temperature, water content and other factors. The fitting curves for each specimen are illustrated in Figure 5-7 with the data together. It seems that the creep rate differs from one location to another. However, because of the lack of an extensive test database the results should be considered as preliminary ones.

From the long-term creep tests, the main observations are summarised as follows:

- The Callovo-Oxfordian clay rock creeps under very low loads of 2 – 3 MPa indicating absence of a lower creep limit.
- Total deformation increases with increasing depth, but the pure creep strains and the creep rates of the specimens from the different depths are similar. This means that according to the long-term creep behaviour, the investigated region of the clay rock is homogeneous.
- Total strains of the large specimens of 100 mm diameter and 200 mm length are higher than those of the small ones of 45 mm diameter and 90 mm length. However, the pure creep strains and the creep rates are similar, independent of specimen size. This means, the scale effect on the creep behaviour of the clay rock is negligible.
- Total deformation perpendicular to the bedding plane is larger than parallel to the bedding. However, no significant differences in creep deformation and creep rate were found for the both loading directions.
- Creep deformation after the stress reduction from 12 MPa down to 10 MPa can recover again after several days.

- Desaturation of the clay specimens exposed to the room air with relative humidity of 24 % at 15 MPa leads to a rapid increase of the compressive deformation (shrinkage) with a large magnitude of 0.3 %.
- Over the creep duration of several months, quasi - steady state creep seems to be reached beyond the transient creep. A linear relation between the quasi - steady state creep rate and the stress was found, but the creep parameter slightly depending on the origin of the rock.

In the literature /ISM 90/, /MIT 92/, /CRI 98/, the creep behaviour of clays are critically reviewed. A very limited amount of laboratory test data is available on the creep behaviour of stiff clays or clay rocks. Because most of the creep tests lasted for short periods of days to months, steady state creep of clay rocks was hardly observed in laboratory, even on the specimens from the Callovo-Oxfordian argillites /LEB 00/, /SU 99/, /HOT 00b/. Because the steady state creep is of most important for characterising the long-term behaviour of the argillites, more longer creep tests are required to validate the observations made by GRS. In addition, mechanisms of the creep in the clay rock are to be investigated to build a solid theoretical foundation, as it was done for rock salt /CRI 98/.

## **5.2 Relaxation Behaviour**

### **5.2.1 Testing Method**

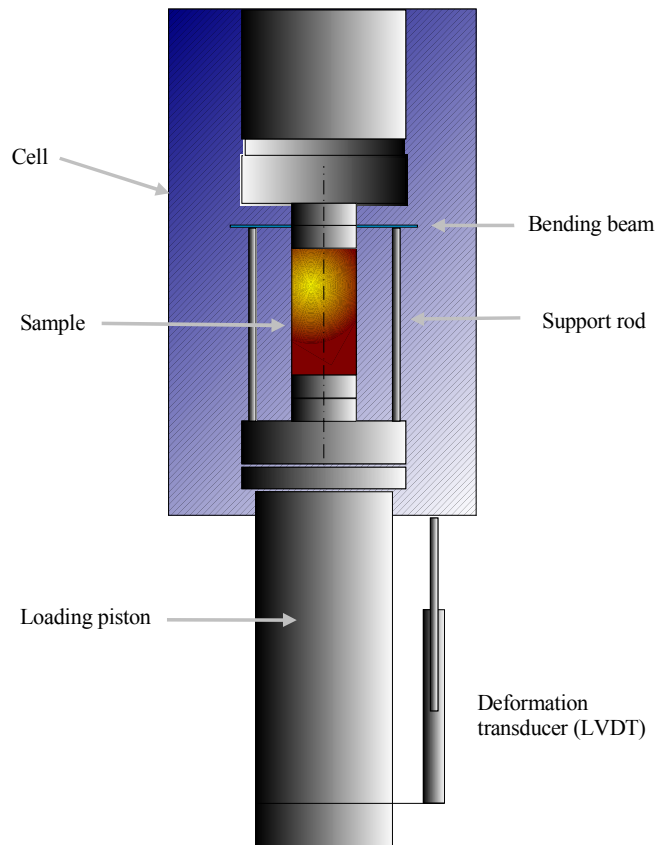
Uniaxial relaxation tests were carried out in combination with the uniaxial compression tests on saturated and air-dried specimens in GRS's triaxial machine (section 4). Generally, relaxation tests are difficult to perform since the condition of null-deformation ( $\dot{\epsilon} = 0$ ) is very delicate to be realized /HAU 91/; /CRI 98/. According to /HAU 91/, a precision of  $\pm 10^{-5}$  is required for the control of the axial length. To meet this requirement in the MODEX-REP laboratory experiments, a special regulating system for controlling null-deformation of specimens during relaxation was developed by GRS.

Figure 5-8 shows the principle of regulating the relaxation condition of null-deformation. The main element of the system is a bending beam which is fixed to the top steel plate. On the joint point between the steel plate and the beam strain gauges are attached. The other end of the beam is supported by a stiff rod fixed on the base plate. As the

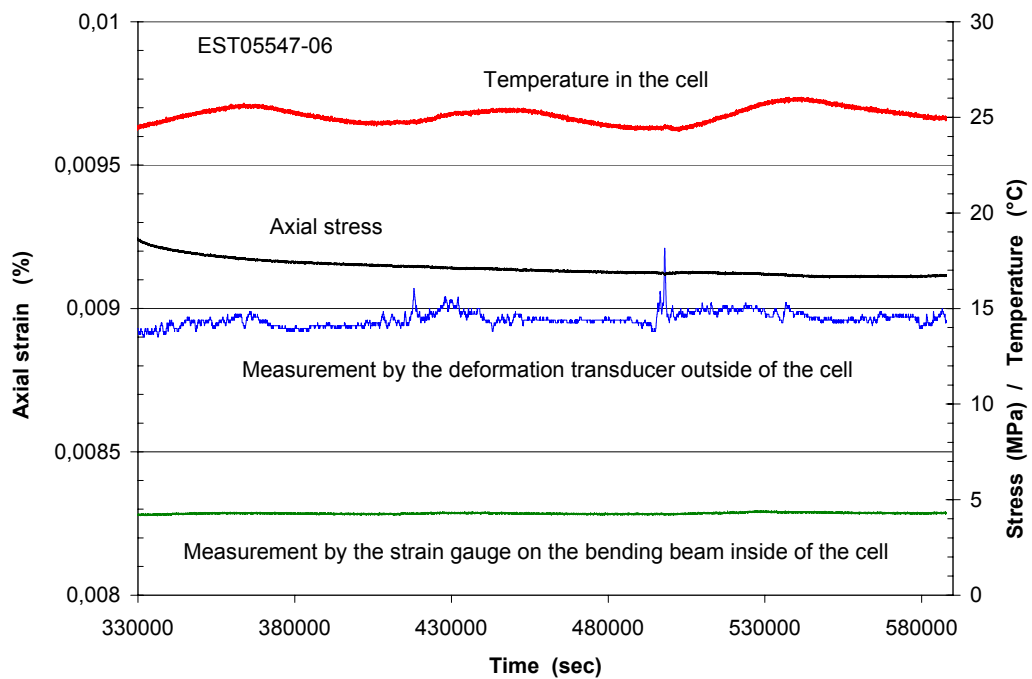
specimen deforms axially, the beam is submitted to the bending load which is concentrated at the joint point where the strain strips are glued. The deformation of the strips generates electronic signals which are output to an electrohydraulic regulator which controls the null-displacement of the loading piston during relaxation.

Figure 5-9 gives an example of the regulated results to gain an insight into the quality of the regulating system. By comparing the regulated data of the null-deformation by using the bending-beam system and the accompanying measurements by using the deformation transducer, it is clearly to be seen that the regulated null-deformation at the achieved strain is rather constant over the whole period of the relaxation phase with a very high accuracy of maximum  $\Delta\varepsilon = \pm 2 \cdot 10^{-7}$ , whereas the scatter of the accompanying measurements by the deformation transducer is  $\Delta\varepsilon = \pm 2 \cdot 10^{-6}$ , one magnitude larger than using the regulating system. The accuracy of the regulation by this system is two magnitudes better than that of  $\pm 10^{-5}$  suggested by /HAU 91/, even the fluctuations of the accompanying measurements by the deformation transducer is about one magnitude less than the requirement range. Because the deformation transducer was positioned outside of the cell, the fluctuations of its accompanying measurements were essentially resulted from the variation of the room temperature which was uncontrolled during the tests. Temperature in the cell was measured between 24 and 26°C (Figure 5-9). A temperature change can lead to thermal expansion of the machine elements and the regulating system, and even the mechanical behaviour of the material depends strongly on temperature, as creep tests have shown. The temperature effects were not investigated in detail in this laboratory programme yet and therefore not considered in the evaluation of the tests.

Four specimens of 40 mm diameter and 80 mm length perpendicular to the bedding plane were tested in uniaxial relaxation, two of them saturated with a water content of 7.1 % and the other two air-dried with the water content of 2.7 - 2.8 %. The specimens were sealed in rubber jackets and steel platens to prevent any change in water content during the tests. The relaxation tests were performed at ambient temperature. Axial load was applied to the specimens with a strain rate of  $6.5 \cdot 10^{-6} \text{ s}^{-1}$  until the desired level was reached and then suddenly stopped ( $\dot{\varepsilon} = 0$ ). The time dependent relaxation of the axial stress was measured. Each relaxation phase lasted about three days.



**Figure 5-8** Principle of maintaining null-deformation of specimen in a relaxation test



**Figure 5-9** Regulation accuracy of null-deformation of specimen EST05547-06 in the uniaxial relaxation test

## 5.2.2 Results

The starting points of the axial stress, the achieved axial strains and the relaxed stresses after 3 days for each relaxation phase are summarised in Table 5.2. According to the starting stress, the tests were divided into two groups, each of which was composed of one saturated and air-dried specimen. In the first group, the relaxation started at about 5 and 15 MPa while in the second group it started at about 10 and 20 MPa.

**Table 5.2** Results of the relaxation tests on the specimens from the Callovo-Oxfordian argillites at MHM-URL

Specimen	Water content w (%)	Starting stress $\sigma_0$ (MPa)	Strain $\varepsilon_0$ (%)	Stress (3 days) $\sigma_{3d}$ (MPa)	Relaxed stress ( $\sigma_0 - \sigma_{3d}$ ) (MPa)
EST05677-02	7.1	4.7	0.17	3.22	1.48
	7.1	14.6	0.49	10.89	3.71
EST05677-04	2.8	5.0	0.19	3.34	1.66
	2.8	15.0	0.53	12.13	2.87
EST05677-03	7.1	9.7	0.37	6.26	3.44
	7.1	19.7	0.74	15.33	4.37
EST05547-06	2.7	10.0	0.45	7.67	2.33
	2.7	20.3	0.89	16.66	3.64

The relaxation results are shown in Figure 5.10 for the first group and in Figure 5-11 for the second group, respectively, in which the time dependent relaxation behaviour of the clay rock in saturated and air-dried conditions are compared. It is obvious that the stress decreases with time for both the saturated and air-dried specimens. A “steady state relaxation”, i.e. relaxation with a constant stress rate (slope of the stress-time curve) can not be observed. The relaxation curves do not cease after 3 days. This means that no creep limit ( $\dot{\varepsilon} = 0$  and  $\dot{\sigma} = 0$ ) was reached during the period of the relaxation time. On the other hand, the reduction of the stress in the saturated conditions was faster than in the air-dried conditions, as shown in Figure 5-12, in which

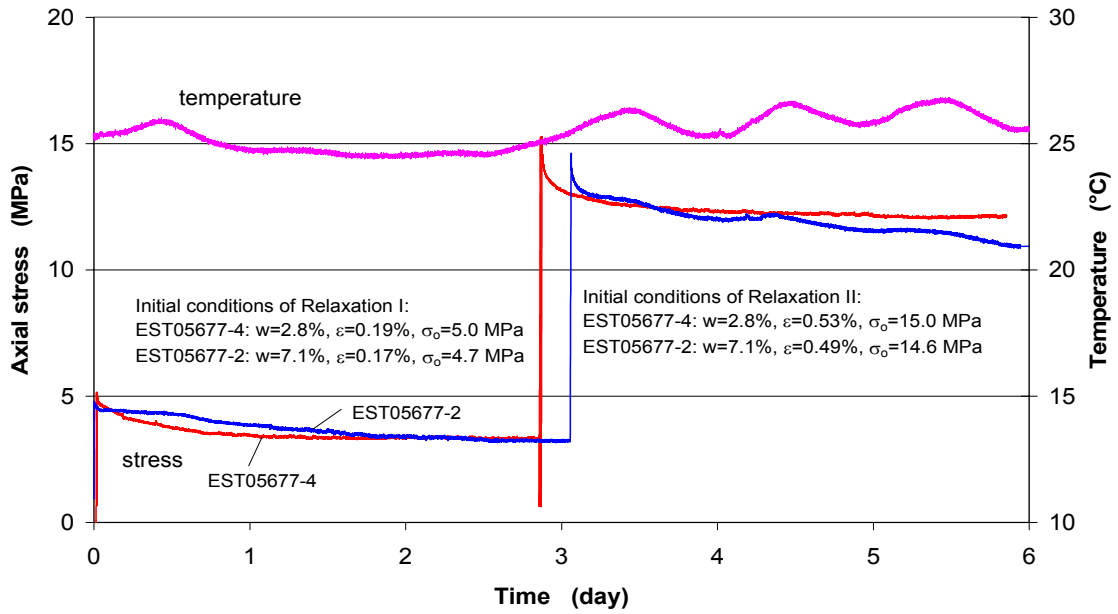


**Figure 5-10** Results of the uniaxial relaxation tests on the specimens EST05677-2 and EST05677-4, starting at 5 and 15 MPa

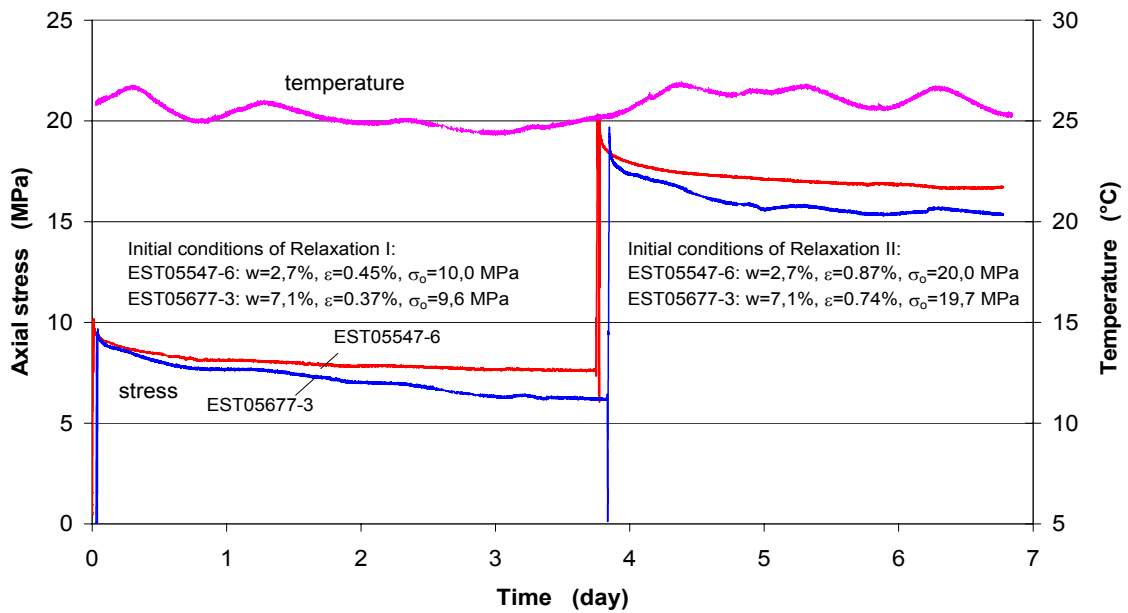


**Figure 5-11** Results of the uniaxial relaxation tests on the specimens EST05677-3 and EST05547-6, starting at 10 and 20 MPa

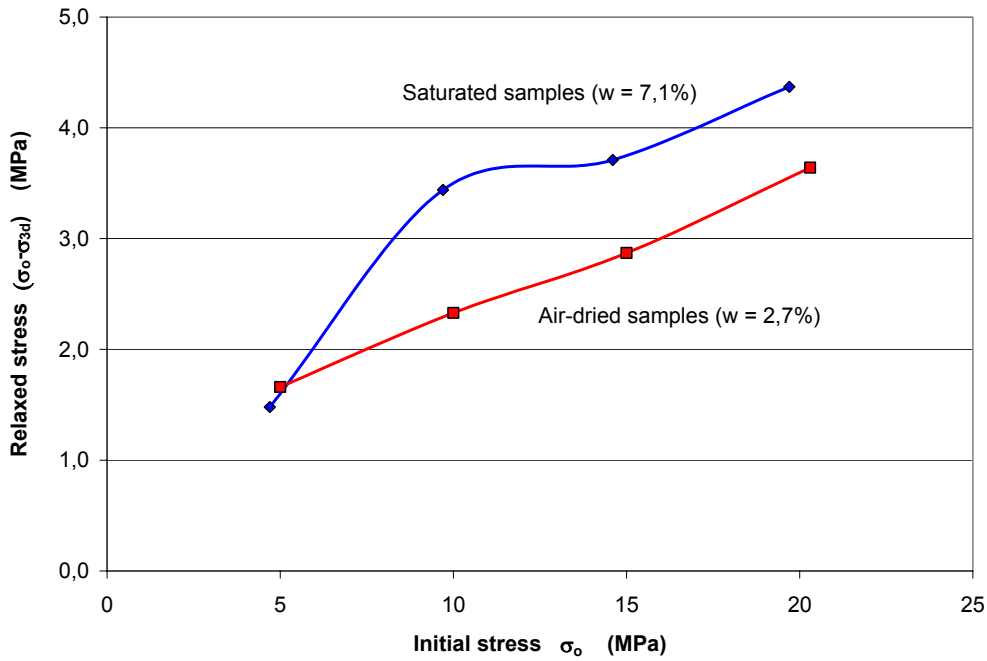


**Figure 5-12** Relaxed stress after 3 days as a function of the starting stress

the relaxed stress after 3 days ( $\sigma_0 - \sigma_{3d}$ ) is given as a function of the starting stress for the saturated and the air-dried conditions. The relaxed stress increases with increasing the starting stress of the relaxation or with increasing the axial deformation. From the Figures 5.10 and 5.11 it is also to be seen that the relaxation of the air-dried specimens is nearly independent on the periodic change of the temperature in the cell whereas the fluctuations of the relaxation curves of the saturated specimens are correlated to the temperature change. As temperature raised, the stress increased.



## 6 Summary

The REP experiment will be conducted in the main shaft of the Meuse/Haute-Marne Underground Research Laboratory (MHM-URL) in Eastern France in order to investigate the hydromechanical response of the Callovo-Oxfordian argillites to shaft sinking. For modelling the coupled hydromechanical processes, respective material parameters are required. A laboratory test programme was performed by GRS within the MODEX-REP project including measurements of the petrophysical properties, permeability tests for characterising the hydraulic behaviour, uniaxial and triaxial compression tests for characterising the short-term mechanical behaviour, and uniaxial creep and relaxation tests for characterising the long-term behaviour of the clay rock.

The testing material was taken from various depths between 434 and 506 m of the borehole EST205 drilled at the axis of the auxiliary shaft of the MHM-URL. Generally, the clay rock is a very compact material with relatively homogeneous structure and with insignificant bedding planes. The mean values of the petrophysical properties measured are as follows: grain density of 2.70 g/cm<sup>3</sup>, bulk density of 2.41 g/cm<sup>3</sup>, dry density of 2.25 g/cm<sup>3</sup>, porosity of 16.8 % and water content of 7.28 %.

- Permeability

Gas permeability of the rock was measured on the wet and saturated and on dried specimens under confining pressures up to 16 MPa. The gas permeability of the dried specimens parallel to the bedding plane varied between 8·10<sup>-19</sup> and 1·10<sup>-17</sup> m<sup>2</sup> for low confining pressures of  $p_c = 2 - 3$  MPa and  $k = 5 \cdot 10^{-19} - 8 \cdot 10^{-19}$  m<sup>2</sup> for high confining pressures of  $p_c = 14 - 16$  MPa, while the gas permeability of the dried specimens perpendicular to the bedding was determined to  $k = 6 \cdot 10^{-20} - 3 \cdot 10^{-19}$  m<sup>2</sup> for the low confining pressures of  $p_c = 2 - 3$  MPa and  $k = 4 \cdot 10^{-20} - 1 \cdot 10^{-19}$  m<sup>2</sup> for the high confining pressures of  $p_c = 14 - 16$  MPa. That means, in the testing range the permeability perpendicular to the bedding plane is about one order of magnitude lower than that parallel to the bedding. The dependence of the gas permeability on the confining pressure, however, is not very significant. The mean values of gas permeability of the specimens are given as follows:  $k = k_0 (p_c / p_0)^{-n}$ , where  $p_0 = 1$  MPa, and  $k_0 = 1.5 \cdot 10^{-19}$  m<sup>2</sup> and  $n = 0.2$  for the permeability perpendicular to the bedding and  $k_0 = 6 \cdot 10^{-18}$  m<sup>2</sup> and  $n = 0.8$  for the permeability parallel to the bedding. Additionally, an increase in water content from 0 % to 4.5 % leads to a decrease of the gas

permeability from about  $10^{-18} \text{ m}^2$  to  $10^{-21} \text{ m}^2$  in the direction parallel to the bedding and from about  $10^{-19} \text{ m}^2$  to  $10^{-22} \text{ m}^2$  in the direction perpendicular to the bedding.

- Short-term compressive behaviour

The uniaxial compression tests have shown that the clay specimens desaturated from the water content of 7.1 % to 2.7 % exhibit a higher uniaxial compressive strength of  $\sigma_c \approx 41 \text{ MPa}$  with an associated maximum strain of  $\varepsilon_{max} \approx 2 \%$  in comparison to the saturated ones with  $\sigma_c \approx 24 \text{ MPa}$  with  $\varepsilon_{max} \approx 1 \%$ . Young's modulus measured on the unloading paths in the uniaxial compression tests increases from  $\sim 5500 \text{ MPa}$  to  $\sim 7500 \text{ MPa}$  with increasing applied stress from 2 MPa to 20 MPa, independent on the water content. Additionally, the elastic modulus determined in the uniaxial multistage creep tests is slightly lower than that determined in the uniaxial compression tests. On the other hand, the elastic stiffness depends on the loading direction. Young's modulus parallel to the bedding is up to 1.5 times larger than that perpendicular. It is also found from the unloading-reloading cycles carried out in the creep tests that Young's modulus of the small specimens (D45/L90 mm) is about two times higher than that of the large ones (D100/L200 mm).

In order to characterise damage, failure and residual strength of the clay rock, multistage triaxial compression tests were carried out on the initially saturated specimens oriented perpendicular to the bedding plane in undrained conditions. Different confining pressures of 1 – 16 MPa were chosen to correspond to in-situ conditions. The clay specimens show yield behaviour followed by strain hardening. The onset of dilatancy was prior but near to failure. The values of peak strength and residual strength determined in the multistage tests are in a good agreement with those obtained by the traditional testing methods. Based on the test data, the strength parameters in the Hoek-Brown and Mohr-Coulomb failure criterion were estimated for the argillites in the rheological zone B' of MHM-URL:

Failure criterion	Hoek-Brown	Mohr-Coulomb
	$\sigma_1 = \sigma_3 + (m \cdot \sigma_c \cdot \sigma_3 + s \sigma_c^2)^{1/2}$	$\tau = \sigma \cdot \tan \varphi + c$
Peak strength	$s = 1, m = 2.5, \sigma_c = 25 \text{ MPa}$	$c = 9.0 \text{ MPa}, \varphi = 19^\circ$
Residual strength	$s = 0, m = 2.5, \sigma_c = 20 \text{ MPa}$	$c = 4.2 \text{ MPa}, \varphi = 19^\circ$

- Long-term creep behaviour

Uniaxial creep tests were conducted in creep rigs at ambient temperature. Axial load was applied stepwise from 2 MPa to 15 MPa on the initially saturated specimens isolated against air, oriented perpendicular and parallel to the bedding plane. Two specimen sizes of D100/L200 mm and D45/L90 mm were tested. The duration of each creep phase varied from about one to seven months. The main observations are:

- The Callovo-Oxfordian clay rock creeps under very low loads of 2 – 3 MPa indicating absence of a lower creep limit.
- Total deformation increases with increasing depth, but the pure creep strains and the creep rates of the specimens from the different depths are similar. This means that according to the long-term creep behaviour, the investigated region of the clay rock is homogeneous.
- Total strains of the large specimens (D100/L200 mm) are higher than those of the small ones (D45/L90 mm). However, the pure creep strains and the creep rates are similar, independent of specimen size. This means, the scale effect on the creep behaviour of the clay rock is negligible.
- Total deformation perpendicular to the bedding plane is larger than parallel to the bedding. However, no significant differences in creep deformation and creep rate were found for the both loading directions.
- Creep deformation after the stress reduction from 12 MPa down to 10 MPa can recover again after several days.
- Desaturation of the clay specimens exposed to the room air with relative humidity of 24 % at 15 MPa leads to a rapid increase of the compressive deformation (shrinkage) with a large magnitude of 0.3 %.
- Over the creep duration of several months, quasi - steady state creep seems to be reached beyond the transient creep. A linear relation between the quasi - steady state creep rate and the stress was found, but the creep parameter slightly depending on the origin of the rock.

Some of the above conclusions are to be validated in further experiments, especially the observations of the steady state creep and the effects of desaturation as well as resaturation.

- Long-term relaxation behaviour

Using the high-precision regulating system developed by GRS to maintain the condition of null-deformation in relaxation tests, the uniaxial relaxation tests were performed on the saturated and air-dried specimens at ambient temperature. The relaxation started at different stresses of about 5 to 20 MPa. Under the same conditions, the axial stress in the saturated specimens relaxed faster than observed at the air-dried ones. The relaxed stress increases with an increase of the starting stress and hence with an increase of the axial deformation. Relaxation did not cease after 3 days for the saturated and air-dried conditions.

## 7 References

- /AND 97/ ANDRA: State of knowledge and experimental program, Underground Research Laboratory. East of France, 1997.
- /AND 99/ ANDRA: REFERENTIEL GEOLOGIQUE DU SITE DE L'EST. A RP ADS 99-005, 1999.
- /AND 00/ ANDRA: Experimental programme at the Meuse/Haute-Marne Underground Research Laboratory.- A short view. June 2000, C RP ASRP 2000 – 2006, 2000.
- /AND 01/ ANDRA: Laboratoire de Recherche Souterrain Meuse / Haute-Marne, Lot 3 – Forages D'investigation Geologique Complementaire – Rapport de Synthese. DRP 0ANT 01-022, 2001.
- /BRO 97/ Bro, A.: Analysis of Multistage Triaxial Test Results for a Strain-Hardening Rock. Int. J. Rock Mech. Min. Sci. Vol. 34, No 1. 143-145, 1997.
- /CRI 98/ Cristescu & Hunsche, U.: Time Effects in Rock Mechanics. – Series: Materials, Modelling and Computation. John Wiley & Sons, Chichester (UK), 1998.
- /GAS 00/ Gasc-Barbier, M; Cosenza, P.; Ghoreychi, M.; Chancole, S.: Laboratory Experiments on Swelling-Shrinkage of Deep Clays under Triaxial Stress. EUROCK 2000 symposium, Aachen 27.-31. March 2000, pp. 705-710.
- /HAU 91/ Haupt, M.: A Constitutive Law for Rock Salt Based on Creep and Relaxation Tests. Rock Mechanics and Rock Engineering. (1991) 24, pp.179-206.
- /HEI 88/ Heitz, J.F.; Haudeville, A.; Hoteit, N.: Geomechanical spectrum of argillaceous rocks. The Geotechnics of Hard Soils – Soft Rocks, Evangelista & Picarelli (eds), 1998 Balkema, Rotterdam, 1988.
- /HOR 96/ Horseman, S.T.; Higgo, J.J.W.; Alexander, J.; Harrington, J.F.: Water, Gas and Solute Movement Through Argillaceous Media. Report CC-96/1, 1996.

- /HOT 00a/ Hoteit, N.; Ozanam, O.; Su, K.: Geological Radioactive Waste Disposal Project in France: Conceptual Model of a Deep Geological Formation and Underground Research Laboratory in Meuse/Haute-Marne Site. The 4<sup>th</sup> North American Rock Mechanics Symposium, Seattle, July 31 – August 3, 2000.
- /HOT 00b/ Hoteit, N.; Ozanam, O.; Su, K.; Chiarelli, A.S.: Thermo-hydro-mechanical behaviour of deep argillaceous rocks. The 4<sup>th</sup> North American Rock Mechanics Symposium, Seattle, July 31 – August 3, 2000.
- /ISM 90/ ISMES: Numerical Modelling of the Creep Behaviour of Clays with Emphasis on Tunnels and Underground Openings – A Critical Review of the State-of-the-Art. Nagra, Technical Report 90-02, 1990.
- /ISR 81/ ISRM: Rock Characterization Testing & Monitoring – ISRM Suggested Methods, 1981.
- /JOC 00/ Jockwer, N., Mieke, R. & Müller-Lyda, I.: Untersuchungen zum Zwei-phasenfluss und difusiven Transport in Tonbarrieren und Tongesteinen, GRS-Abschlußbericht. GRS-167, 2000.
- /LEB 00/ Lebon, P.; Ghoreychi, M.: French Underground Research Laboratory of Meuse/Haute-Marne: THM Aspects of Argillite Formation. EUROCK2000, Aachen, 27.-31. March 2000.
- /LEB 96/ Lebon, P.; Hoteit, N.; Trentesaux, C.: Research on the mechanics of clayed rocks in the French programme on radioactive waste disposal in deep geological formations. Rock Mechanics, Aubertin, Hassani & Mitri (eds), Balkema, Rotterdam, 1996.
- /MIT 92/ Mitchell, J.K.: Charakteristiks and Mechanisms of Clay Creep Rupture. In: cms workshop lectures, Vol. 4: Clay-Water interface and its rheological implications, Clay Mineral Society, 1992., pp. 212-244.
- /OZA 99/ Ozanam, O.; Su, K.: Technical Specifications for E-REP Experiment - Mechanical Response of the Argillite to Shaft Advancement. ANDRA, CCC AGEM99-049/B, 1999.

- /OZA 00/ Ozanam, O.; Su, K.; Hoteit, N.: First in-situ Experiment in the French Underground Laboratory: Vertical Mine-by-Test in the Main Shaft. WM'00 Conference, Tucson – Arizona, February 27 – March 2, 2000.
- /REN 00/ Renner, J., Hettkamp, T. & Rummel, F.: Rock Mechanical Characterization of an Argillaceous Host Rock of a Potential Radioactive Waste Repository. In: Rock Mechanics and Rock Engineering, 33 (3), 153-178, 2000.
- /SU 99/ Su, K.; Ozanam, O.: Rheological model for the Eastern argillites – Summary of status for the rheological studies (Meuse/Haute-Marne site). C RP AGEM 99-061, 1999.
- /SU 02/ Su, K.; Ben Slimane, K.: Introduction of the Meuse/Haute-Marne site and the REP experiment –Part 1 of the MODEX-REP project report. Deliverable 2 & 3 of MODEX-REP (to be appeared).

## List of Figures

Figure 1-1	General view of the MHM-URL in France /ANDRA/ .....	1
Figure 1-2	Cross section of the Meuse/Haute-Marne site /ANDRA/ .....	2
Figure 1-3	Mineralogy and geomechanical sub-division of the Callovo-Oxfordian formation /ANDRA/ .....	2
Figure 1-4	Schematic of the REP experiment in the main shaft of the MHM-URL /ANDRA/ .....	4
Figure 2-1	Sample EST05481 of the Callovo-Oxfordian argillites from the borehole EST205 in the GRS laboratory under storage conditions and during specimen preparation .....	7
Figure 2-2	Core samples taken from the Callovo-Oxfordian argillites from the borehole EST205.....	8
Figure 3-1	Schematic of the measurement principle and the testing apparatus of gas permeability at GRS geotechnical laboratory in Braunschweig .....	16
Figure 3-2	Permeability of the Callovo-Oxfordian argillites in dependency on flow direction and confining pressure (dry specimens).....	19
Figure 3-3	Gas permeability of the Callovo-Oxfordian argillites in dependency on water content .....	21
Figure 3-4	Comparison in permeability of the Callovo-Oxfordian argillites at MHM-URL with that of the marls and shales Swiss Central Alps /REN 00/ .....	21
Figure 4-1	Triaxial testing machine used at GRS geotechnical laboratory in Braunschweig.....	23

Figure 4-2	Results of uniaxial compression tests on the specimens from the Callovo-Oxfordian argillites at MHM-URL.....	25
Figure 4-3	Young's modulus as a function of axial stress (uniaxial compression tests) .....	26
Figure 4-4	Stress-strain curves obtained from uniaxial creep tests .....	28
Figure 4-5	Young's modulus as a function of axial stress (uniaxial creep tests) .....	28
Figure 4-6	Results of multistage triaxial compression tests on the specimens from the Callovo-Oxfordian argillites at MHM-URL .....	30
Figure 4-7	Volumetric deformations of the specimens tested in the first confining stage .....	33
Figure 4-8	Peak strength and residual strength of the Callovo-Oxfordian argillites at MHM-URL (zone B'), Hoek-Brown failure criterion.....	35
Figure 5-1	Uniaxial testing machines for two and five simultaneous creep tests at GRS geotechnical laboratory in Braunschweig.....	38
Figure 5-2	Group I: Two simultaneous uniaxial creep tests on the specimens EST05582-01 and EST05630-01 at ambient temperature with four succeeding stresses .....	47
Figure 5-3	Group II: Two simultaneous uniaxial creep tests on the specimens EST05481-01 and EST05671-01 at ambient temperature with six succeeding stresses.....	49
Figure 5-4	Group III: Two simultaneous uniaxial creep tests on the specimens EST05677-01 and EST05751-01 at ambient temperature with two succeeding stresses.....	48

Figure 5-5	Group IV: Five simultaneous uniaxial creep tests on the specimens EST05630-02, EST05582-02, EST05582-03, EST05671-02 and EST05671-03 at ambient temperature with four succeeding stresses .....	53
Figure 5-6	Scale effect on the creep behaviour .....	54
Figure 5-7	Quasi - steady state creep rates as a function of the applied stresses determined on specimens from the Callovo-Oxfordian argillites at ambient temperature .....	54
Figure 5-8	Principle of maintaining null-deformation of specimen in relaxation test .....	58
Figure 5-9	Regulation accuracy of null-deformation of the specimen EST05547-06 in the uniaxial relaxation test .....	58
Figure 5-10	Results of the uniaxial relaxation tests on the specimens EST05677-2 and EST05677-4, starting at 5 and 15 MPa .....	60
Figure 5-11	Results of the uniaxial relaxation tests on the specimens EST05677-3 and EST05547-6, starting at 10 and 20 MPa .....	60
Figure 5-12	Relaxed stress after 3 days as a function of the starting stress .....	61

## List of Tables

Table 1.1	General mechanical characteristics of the Callovo-Oxfordian formation.....	3
Table 2.1	Core samples taken from the Callovo-Oxfordian argillites at MHM-URL and test plan for laboratory tests .....	9
Table 2.2	Measurements of the grain density on powder specimens from the Callovo-Oxfordian argillites at MHM-UTRL using Beckmann' Pycnometer.....	13
Table 2.3	Petrophysical properties of the Callovo-Oxfordian argillites at MHM-URL.....	14
Table 3.1	Results of gas permeability tests on the Callovo-Oxfordian argillites at MHM-URL .....	18
Table 4.1	Results of the multistage triaxial compression tests on specimens from the Callovo-Oxfordian argillites in zone B' at MHM-URL.....	34
Table 4.2	Strength parameters for the Callovo-Oxfordian argillites in zone B' at MHM-URL (based on the GRS-data and ANDRA-data).....	36
Table 5.1	Overview of the uniaxial creep tests on the specimens from the Callovo-Oxfordian argillites at MHM-URL.....	40
Table 5.2	Results of the relaxation tests on the specimens from the Callovo-Oxfordian argillites at MHM-URL.....	59

**Gesellschaft für Anlagen-  
und Reaktorsicherheit  
(GRS) mbH**

Schwertnergasse 1  
**50667 Köln**  
Telefon +49 221 2068-0  
Telefax +49 221 2068-888

Forschungsinstitute  
**85748 Garching b. München**  
Telefon +49 89 32004-0  
Telefax +49 89 32004-300

Kurfürstendamm 200  
**10719 Berlin**  
Telefon +49 30 88589-0  
Telefax +49 30 88589-111

Theodor-Heuss-Straße 4  
**38122 Braunschweig**  
Telefon +49 531 8012-0  
Telefax +49 531 8012-200

**[www.grs.de](http://www.grs.de)**